Development of a tracking compound parabolic collector for a solar-driven diffusion absorption cycle

TP Kitching

orcid.org/0000-0003-1666-7240

Dissertation submitted in fulfilment of the requirements for the degree *Master of Engineering* in Mechanical Engineering at the North-West University

Supervisor: Prof CP Storm

Graduation May 2018

Student number: 22800239

NWU ®

NORTH-WEST UNIVERSITY
NOORDWES-UNIVERSITEIT
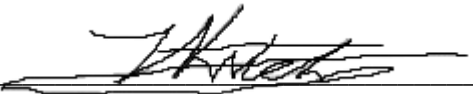UNIBESITI YA BOKONE-BOPHIRIMA

Declaration

I, **TERTIUS KITCHING**, declare that this report is a presentation of my own original work.

Whenever contributions of others are involved, every effort was made to indicate this clearly, with due reference to the literature.

No part of this work has been submitted in the past, or is being submitted, for a degree or examination at any other university or course.

Signed on this, 5th day of December 2017, in Potchefstroom.

TP KITCHING

Abstract

In an aqua ammonia absorption refrigeration system, the heat required by the generator can be delivered by a renewable source, such as solar energy. A compound parabolic collector (CPC) can deliver medium to high temperatures with relatively low heat loss, making it a good candidate for use in such a system. A CPC has been designed that can provide a temperature of 90°C to the bubble-pump generator of an in-development aqua ammonia absorption refrigeration system.

Previous studies in this field focused mainly on stand-alone CPCs, as well as stationary CPCs specifically for use in solar-driven absorption systems. From the literature it was gathered that an East-West orientation of a collector results in more absorbed energy, and that sun-tracking also increases the amount of energy absorbed. No literature was found regarding the use of a sun-tracking CPC for use in a solar-driven absorption system.

A mathematical model was developed to predict the amount of useful energy gained with a particular design. The model included determining the path of the sun in the sky throughout the year, determining a CPC profile, gathering solar radiation data, and determining the thermal performance of the CPC. The modelled sun-tracking CPC with a concentration ratio of 2.09, receiver radius of 16 mm, and total collector area of 9.84 m^2, was then constructed and tested.

Testing took place from 29 March 2017 to 30 March 2017 and showed that, on a cloudy day, a maximum temperature of 109°C was achieved. The results translate to an actual useful energy gain of up to 4462.33 W, varying with weather conditions. Compared to the theoretical useful energy gain of 3681.45 W for a cloudy day, and 4806.83 W for a clear sky day, the actual results correlate well with these figures.

As the collector produced temperatures above 90°C, it would be able to provide the bubble-pump generator with the heat it needs to drive the aqua ammonia absorption refrigeration system.

Recommendations include converting the tracking mechanism to an electronic system, as well as using an electronic system to control the flow rate through the collector. It is also recommended that any future measurements on the collector be taken only when the entire refrigeration system is fully assembled.

Keywords: CPC; compound parabolic collector; aqua-ammonia; sun-tracking; escapement, absorption refrigeration.

Acknowledgements

The author would like to acknowledge the following individuals for their support during this study.

My sincere gratitude to Professor Chris Storm of the North-West University for his leadership and guidance. You truly are the most helpful and knowledgeable lecturer that a student could hope for.

To my love, Marica, your support and encouragement has been as invaluable as you are irreplaceable. I will treasure you always.

To my parents, Alet and Petrus, your emotional and financial support have opened countless doors for me. You have made me the person I am today.

I am beholden to the Lord Jesus Christ, who has granted me patience, perseverance and everlasting life. By myself, this would have been impossible. But with You, all things are possible.

Table of Contents

List of Figures

List of Tables

Nomenclature

Symbols

α	Solar altitude angle	[°]
α_r	Absorptivity of receiver	
γ	Correction factor for diffuse radiation	
δ	Solar declination angle	[°]
ε_r	Emissivity of receiver	
Θ_a	Acceptance angle	[°]
Θ_i	Incident angle	[°]
Θ_r	Reflected angle	[°]
Θ_t	Refracted angle	[°]
ρ	Mirror reflectivity	
T_{cover}	Transmissivity of cover	
T_{CPC}	Effective transmissivity	
A_a	Total aperture area	[m^2]
A_{CPC}	Aperture area of one CPC	[m^2]
A_r	Total receiver area	[m^2]
a	Aperture size	[mm]
a'	Receiver size	[mm]
C	Concentration ratio	
c_p	Specific heat	[J/kgK]
D_i	Inner diameter of receiver	[mm]
D_o	Outer diameter of receiver	[mm]
F'	Collector efficiency factor	
F_R	Heat removal factor	
h	Hour angle	[°]
h_f	Convective heat transfer coefficient of fluid	[W/m^{2}K]
G_D	Diffuse radiation	[W/m^2]
G_t	Total incident radiation	[W/m^2]
k	Thermal conductivity of receiver	[W/mK]
k_f	Thermal conductivity of fluid	[W/mK]
L	Length of CPC	[mm]
L_{at}	Local latitude	[°]
LiBr	Lithium-Bromide solution	

m_{dot}	Mass flow	[kg/s]
N	Day of the year	
n	Average number of reflections	
n_d	refractive index of medium	
NH_3	Ammonia	
Nu	Nusselt number	
n_i	Refractive index of initial medium	
n_t	Refractive index of final medium	
r	Receiver radius	[mm]
Q_u	Useful energy gain	[W]
S	Absorbed solar radiation	[W/m^2]
T_a	Ambient temperature	[°C]
T_i	Inlet temperature	[°C]
T_o	Outlet temperature	[°C]
U_L	Overall heat loss coefficient	[W/m^{2}K]
y	Y Cartesian coordinate	
Z	Z Cartesian coordinate	
z	Solar azimuth angle	[°]

Abbreviations

Br	Bromide
CO_2	Carbon dioxide
COP	Coefficient of performance
CPC	Compound parabolic concentrator
ETC	Evacuated tube collector
FPC	Flat plate collector
H_2O	Water
Li	Lithium
NH_3	Ammonia
PTC	Parabolic trough collector
PV	Photo-voltaic
PVGIS	Photovoltaic Geographical Information System
U.S.	United States (of America)

1 Introduction

1.1 Background

In modern times heating and cooling is achieved by using electricity that is mainly produced from fossil fuels, such as coal and oil. These fuels are in limited supply and the burning of them causes widespread pollution. The construction of coal power plants is also costly and time-consuming, which may lead to a country not being able to keep up with the rate of increase of the electricity demand.

There are, however, alternative means to provide heating and cooling. An absorption cycle such as in Figure 1, though typically used for refrigeration, can simultaneously be used for heating. This cycle is based upon the principle that certain liquids have a great affinity for absorbing large amounts of certain vapours. According to Stoecker and Jones (1983:347), the liquid-vapour pairs that are commonly used include LiBr-water and aqua-ammonia (i.e. a water and ammonia mixture). Stoecker and Jones (1983:347) also explain the working of an aqua-ammonia cycle, stating that an external heat source is added to the generator, causing ammonia vapour to be produced from a strong solution of NH_3 along with water vapour, which is removed in the rectifier, allowing the ammonia to pass through a water-cooled heat exchanger, known as the analyzer, which condenses some water-rich liquid that returns to the rectifier.

The ammonia then condenses in the condenser and enters the evaporator after its pressure and temperature is adjusted by a throttle valve. The refrigerant then absorbs enough heat from the evaporator to leave as a saturated vapour and is then absorbed by the weak solution of NH_3, which is sprayed into the absorber after leaving the generator and passing through a heat exchanger. A strong solution of NH_3 then leaves the absorber and is pumped through the same heat exchanger that the weak solution passed through, and then enters the generator.

Van Der Walt (2012:3) states that in order to circulate the refrigerant, a diffusion absorption cycle can be used instead of a regular pump-driven absorption cycle. This cycle induces circulation by injecting an auxiliary non-reactive gas such as hydrogen or helium into the evaporator in order to lower the pressure of the refrigerant in accordance with Dalton's law of partial pressures, which states that in a mixture of non-reacting gases, the total pressure is equal to the partial pressures of each gas.
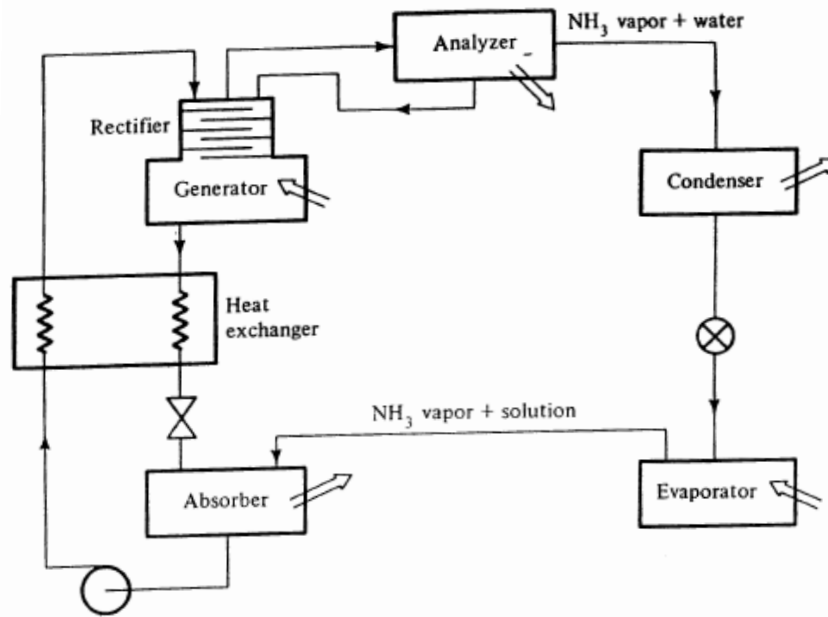
Figure 1: Aqua-ammonia absorption cycle (Stoecker, 1983:348)

Furthermore White (2001:1) states that the need for a mechanical input can be eliminated by using a heat-driven bubble pump, as is illustrated in Figure 2. A bubble pump is a device that consists of a bottom chamber beneath a narrow cylindrical tube. The bottom chamber is filled with a solution, such as in this case NH_3 and water. When heat is applied to the chamber, bubbles begin to form in the solution. The pump is designed is such a way that these bubbles travel up the tube one by one, carrying some of the solution between the bubbles along with them. At the top of the tube, the gas bubbles and solution are separated, as the gas rises further to the condenser, while the solution flows over the side of the tube and is directed to the absorber.

In the case of a NH_3 and water solution, it is important that the heat supplied is such that only the NH_3 will start to boil and release gas bubbles, while the water remains in liquid form. This is to ensure that only ammonia gas rises to the condenser, resulting in a strong solution of NH_3 later on in the cycle. Therefore, because the boiling point of water is 100°C, it is recommended that a lower temperature than this is supplied to the bubble pump.

As an alternative to using an electrical element or bottled gas to supply heat to the generator, solar energy can be used. As can be seen in Figure 3, South Africa's solar resources are among the best in the world. However, once sunlight reaches the atmosphere, some of it is scattered and reaches the earth as diffuse radiation, while the unscattered light is known as direct or beam radiation, according to Kalogirou (2009:91).

To utilize the solar energy, solar collectors which use the thermal energy from sunlight, and photovoltaic (PV) panels which convert the energy from photons into electric potential, can be used. Although there have been many advances in the field of photovoltaics, it is still more expensive than municipal electricity, and as the energy that needs to be provided to the generator must be in the form of heat, it would be inefficient to generate electric energy and convert it to heat, instead of simply generating thermal energy.
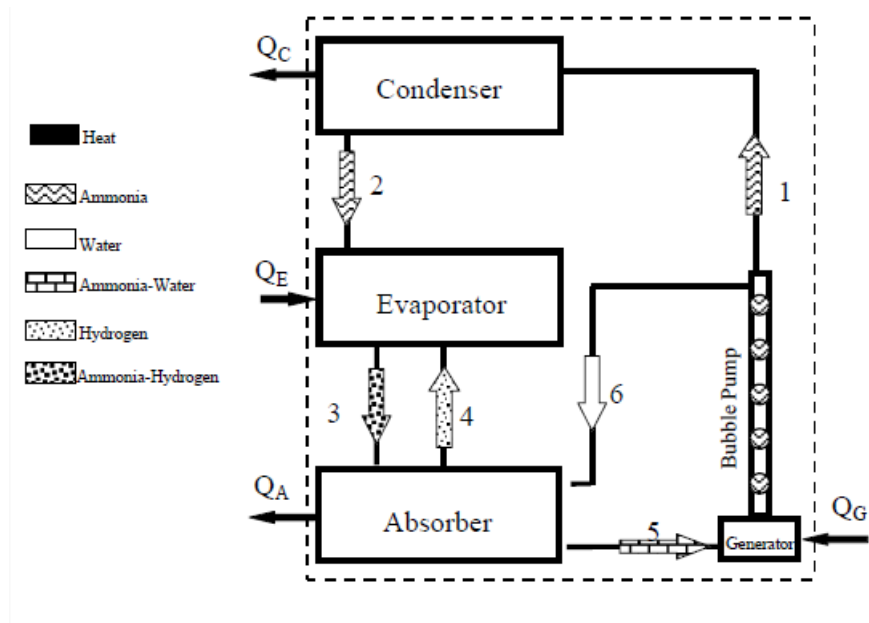
Figure 2: Aqua-ammonia diffusion absorption cycle with bubble pump (White, 2001:5)
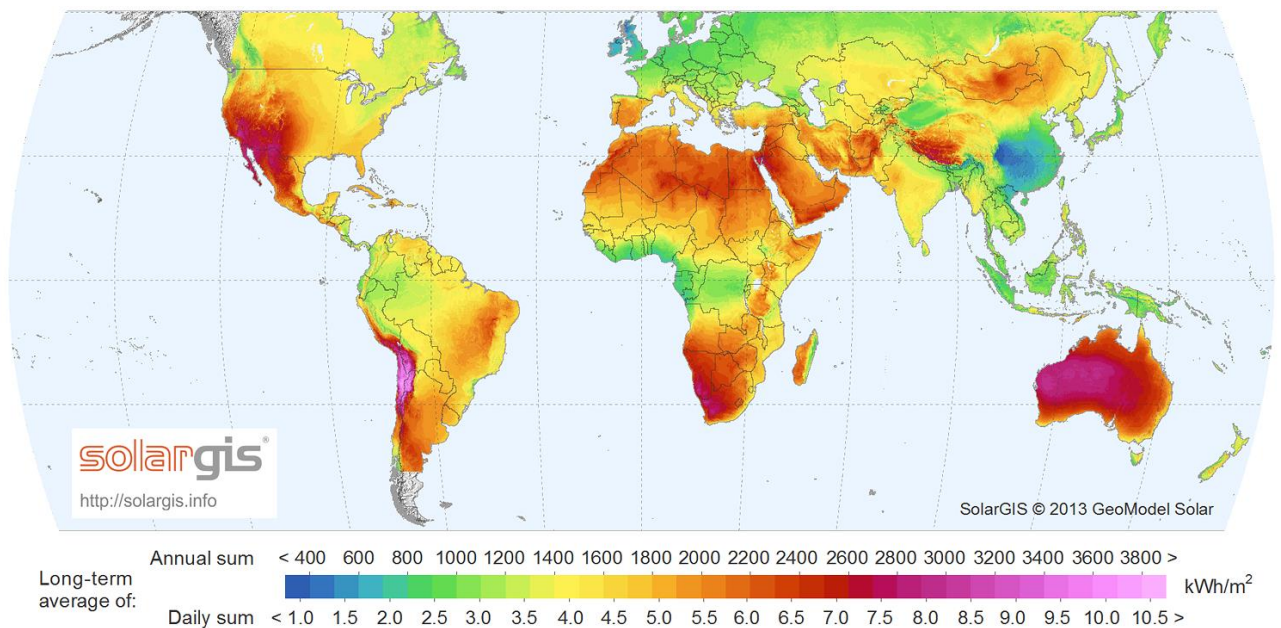
Figure 3: World map of direct normal irradiation (SolarGIS, 2013)

There exist several types of solar collectors, though some are experimental and some, such as Fresnel lenses and parabolic dishes, would be very difficult to implement into a diffusion absorption system, because they require that the points on which they focus rotate with them as they track the sun. Heliostat field collectors would also be unsuitable as they require precision tracking with multiple panels and a large area of collection.

Collectors that could be used include:

- Flat plate collectors (FPCs)
- Evacuated tube collectors (ETCs)
- Parabolic trough collectors (PTCs)
- Compound parabolic collectors (CPCs)

FPCs have a simple configuration, consisting of a covered frame which contains an absorber plate with tubes welded to it, as seen in Figure 4. Kalogirou (2009:123) states that they are relatively inexpensive to manufacture and can collect both diffuse and beam radiation. They are generally used for applications that require relatively low temperatures (up to 80 °C) and would therefore be unsuitable for use in an absorption cycle, unless expensive design choices are made, including highly selective coatings that can increase the temperature to above 100 °C, as noted by Kalogirou (2009:129).
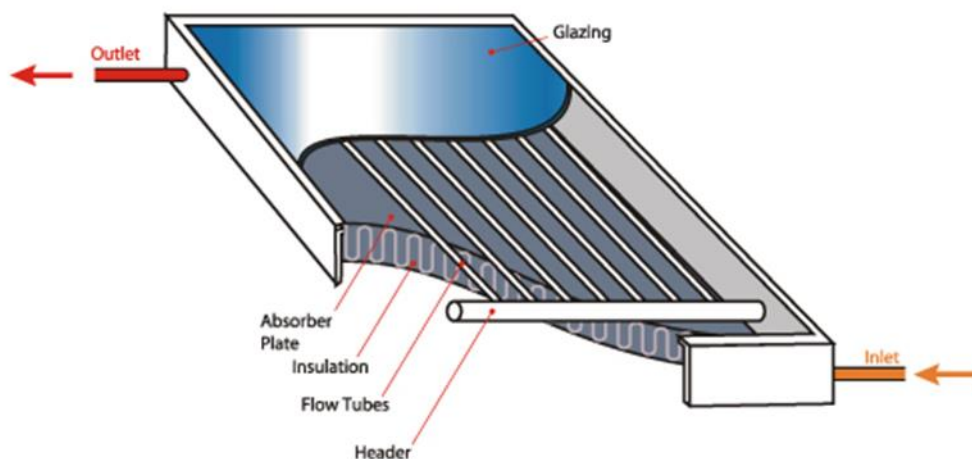
Figure 4: Typical Flat Plate Collector (GGHS, 2011)

ETCs, shown in detail in Figure 5, have a heat pipe inside of a glass tube that is vacuum sealed, which reduces conduction and convection heat loss. The heat pipe contains a heat transfer fluid which evaporates as the pipe heats up and the gas flows to the cooler end of

the pipe where it condenses and transfers heat to the working fluid. The fluid then flows back to the hot end where it is heated again.

Kalogirou (2009:134) states that these collectors are expensive, and though it collects beam and diffuse radiation and temperatures up 200 °C can be achieved, the cost and difficulty in manufacturing vacuum sealed tubes makes this collector unsuitable for the purpose of this study.
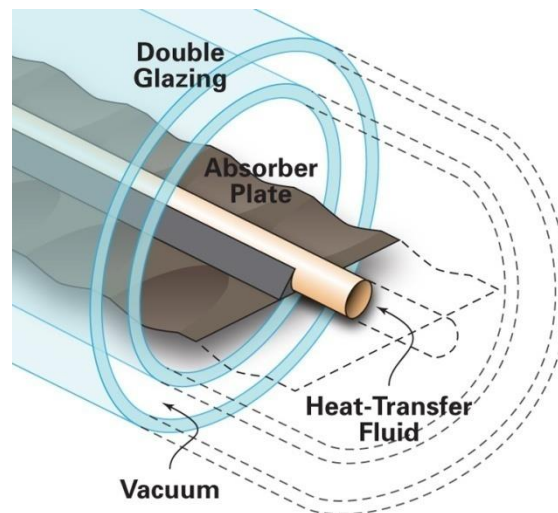
Figure 5: Cross-section of ETC tube (Mehalik, 2009)

PTCs are made by bending a metal sheet in the shape of a parabola with a focus point centred on a black metal tube through which the working fluid flows. Figure 6 shows that the solar radiation falling on the reflector opening area is reflected and concentrated onto the pipe, heating the fluid inside. According to Kalogirou (2009:138) temperatures of up to 400 °C can be reached efficiently. However, PTCs require precise tracking mechanisms, as it cannot collect diffuse radiation and any beam not falling exactly perpendicular to the reflector opening, will not be absorbed. Such tracking mechanisms require constant adjustment and electricity, which strays from what a stand-alone diffusion absorption system would employ.

CPCs work on the same principle as the PTC, except that its parabolic shape is a compound of two parabolas. Winston (2005) explains that this creates an acceptance angle, as seen in Figure 7, which allows the collector to absorb any solar beam with an incidence angle that is within the acceptance angle. This type of collector does not require tracking as the acceptance angle can simply be adjusted to include all angles of solar incidence for a certain geographical location. Concentrating the solar energy leads to less heat loss through the absorber, due to its smaller area. These systems generally have a higher efficiency than

FPCs and PTCs. Kalogirou (2009:131) states that a CPC is generally used for higher temperature applications and this, coupled with no or some tracking, would make the CPC a good candidate for use in a diffusion absorption system.
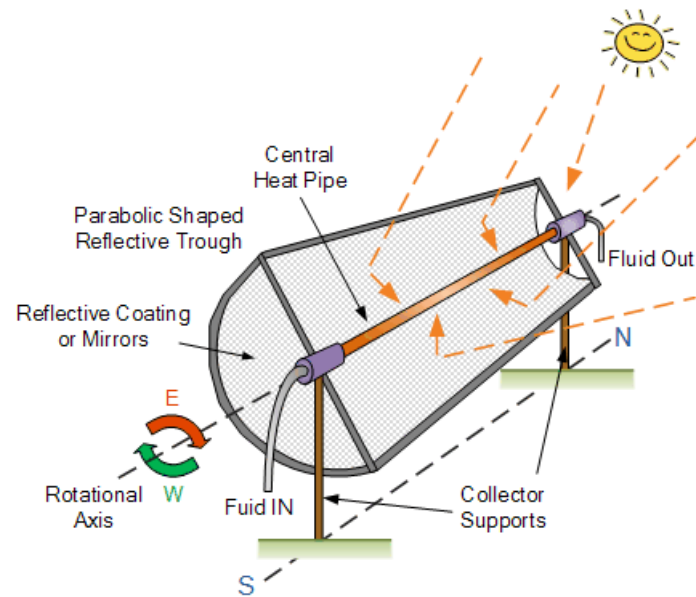
Figure 6: Typical Parabolic Trough Collector (Alternative Energy Tutorials, s.a.)
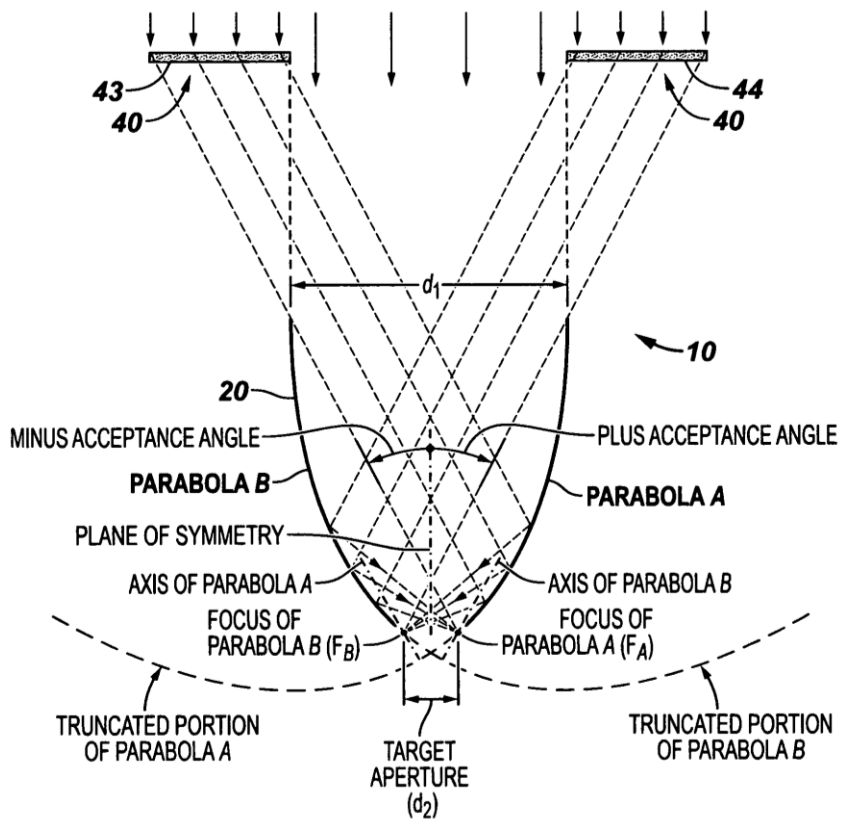
Figure 7: A CPC profile showing acceptance angle (Casperson, 2011)

The problem with solar energy is that solar radiation is not constant, but varies according to the following factors:

- Geographic location;
- Day or night;
- Seasons;
- Weather, including cloud coverage, rain, etc.;
- Local air pollution;
- Solar activity such as sun spots or solar flares; and
- Climate change.

In order to harness solar energy over a period of 24 hours, Potgieter (2013:47) and Kalogirou (2009:275-286) notes that thermal "batteries" can be used. These are a type of heat storage system that utilizes a phase change material, molten salt, or other material that easily absorbs and stores the heat. From there the heat can be transferred to the generator of a diffusion absorption cycle.

Such a system as described above would be able to provide refrigeration and limited heating to rural areas where frequent power outages occur or where the power grid does not reach, such as small farms and isolated homes. Though photo-voltaic solar panels could also be used in such a situation, the technology is as of yet still inefficient, expensive and requires frequent maintenance.

1.2 Problem Statement

An experimental aqua-ammonia diffusion absorption system that is intended for rural domestic use is currently in development. It is, however, only a demo unit for the purpose of concept testing and is not intended for actual domestic use. The entire system is being designed to be contained in a frame that was designed and built to fit on a large trailer so that it can be transported to its destination for testing. It is in need of a renewable energy source that can supply the bubble-pump generator with enough heat to maintain its working temperature at day and night.

1.3 Objective

The aim of this study is to design and construct a compound parabolic solar collector to deliver heat to the generator. The collector must be able to produce a temperature of 90°C and must be able to fit in the available space on the built absorption system frame.

1.4 Scope and Limitations

This study includes the collector design, manufacturing and testing, as well as evaluating the inclusion of solar tracking, the selection of an appropriate heat transfer fluid and the design and selection of other related system components including pumps, piping and valves.

The study does not include the design of the heat storage system or any components of the aqua-ammonia diffusion absorption system itself.

The limitations of this study include the following:

- The geographic location, and thus the solar resource, is limited to Potchefstroom, South Africa.
- The maximum collector area is limited by the size of the built absorption system frame, shown in Figure 8. The frame was designed to allow space for the collector of one side of the angled roof, with the other side being occupied by another component. The roof has an angle of 45° and one side of the roof has a size of 1.06m x 3.78m.
- Multiple studies regarding the other components in the absorption system will take place concurrently with this study. This will impact the design and duration of this study, as constant communication between studies influence the requirements of this design.
- The design is also limited by taking into consideration that the frame must contain all the components of the diffusion absorption system.

1.5 Research Methodology

The procedure that will be followed in this study is stated below:

- Accurate data for solar irradiation and irradiance must be collected for the area of Potchefstroom.
- The orientation of the CPCs must be determined, either N-S with E-W tracking, or E-W with N-S tracking.
- The CPC reflector profile can then be designed.
- The CPC materials must be determined as well as the heat transfer fluid.
- With all the properties in place, the amount of heat that can be absorbed by the collector can be calculated.

- The necessary mass flow of the heat transfer fluid to reach the minimum temperature can be determined, allowing for an appropriate pump to be chosen.
- The tracking mechanism is then designed.
- With all other design finished, the collector mounting to the frame can be designed.
- After ordering parts and materials, the CPC system can be assembled.
- Commence testing and take accurate measurements. Compare these results to the simulated results.
- Meaningful discussions and conclusions can then be made.

Representation of pre-constructed frame.
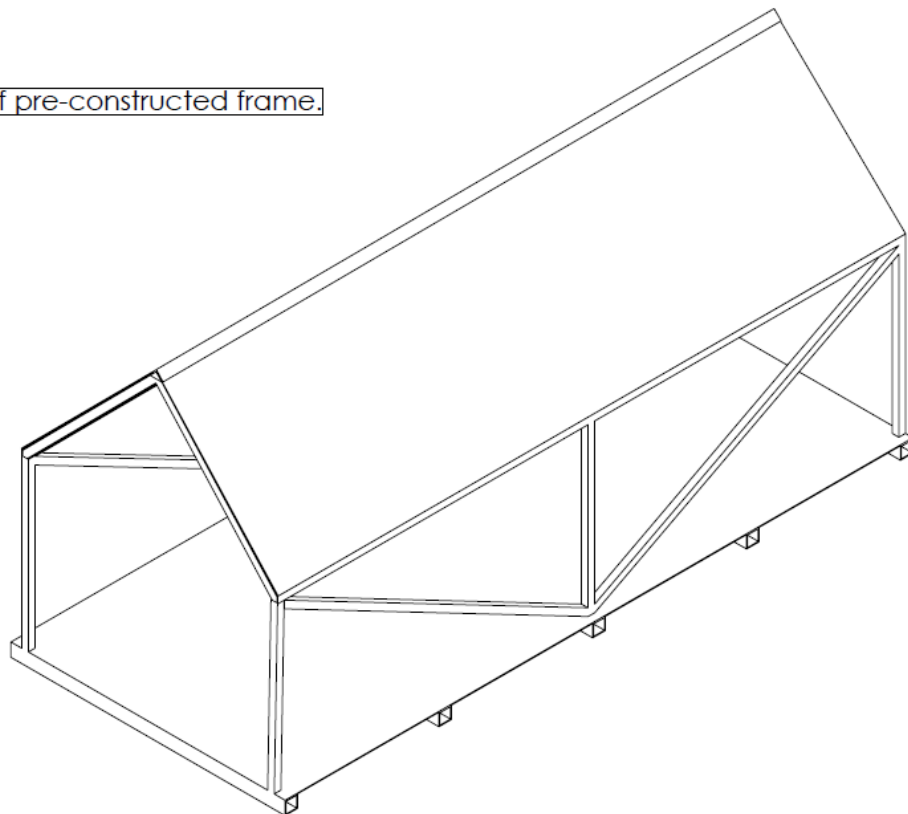
Figure 8: Drawing view of constructed system frame that houses absorption system components

1.6 Summary of Chapters

The following is a summary of the contents of each of the chapters contained in this study.

Chapter 1:

This chapter contains an introduction to the study, including a background and the details surrounding the problem to be addressed by this study.

Chapter 2:

This chapter is a summary of previous studies that have been done in fields relating to this study.

Chapter 3:

This chapter includes the theory and formulas relevant to the content of this study.

Chapter 4:

This chapter describes the mathematical model used to ascertain certain design parameters and predict the results of the eventual design.

Chapter 5:

This chapter describes the design choices and fabrication details related to this study.

Chapter 6:

This chapter describes the experimental setup used to test the design, including the measurement equipment and test procedure.

Chapter 7:

This chapter addresses the results gained from the experiment.

Chapter 8:

This chapter includes the conclusions derived from the results of this study, as well as recommendations for future study on this topic.

2   Literature Survey

In this chapter, previous studies that have investigated the topics applicable to this study is presented. Previous work carried out in this field of study has tended to focus on the following areas:

- Stand-alone CPCs
- Stationary CPCs used in solar-driven absorption systems
- Sun-tracking mechanisms

2.1   Stand-alone CPCs

The compound parabolic concentrator, or CPC, was introduced by Roland Winston in 1974. It is a non-imaging two-dimensional concentrator that consists of a reflector in the shape of two parabolas which axes are inclined at a "half acceptance angle" to the symmetrical axis of the collector. This half acceptance angle is the angle through which a light beam can be rotated while still converging at the absorber. The beams are reflected onto an absorber, the shape of which can vary between flat plates, tubes and wedges, depending on the space available and the need for sun-tracking.

Garrison et al. (1993) expanded on the work done by Winston by integrating another CPC into the absorber. This is done by forming the glass tube of the evacuated tube around the absorber into the CPC profile, further concentrating the light-beams. The reflector is made by evaporating a silver coating onto an interior glass profile. Though the silver would normally oxidize in the air and become less reflective, it is protected from this by the vacuum. The internal reflector profile allows a smaller gap to exist between the outer reflector plate and the absorber. This gap is usually larger when only an evacuated glass tube is used with an outer reflector.

Using this approach, efficiencies of up to 50% were achieved at a temperature of 200°C. This solution allowed for lower heat loss, a higher heat transfer coefficient and, due to only one end of the pipe being fixed, less stress on the vacuum encasement from thermal expansion. This study only evaluated a CPC with a tubular absorber.

Farouk Kothdiwala et al. (1995) focused on a tubular absorber with an evacuated glass envelope surrounding it and an external CPC reflector profile, a practice that, while reducing heat loss, significantly increases optical losses due to the large gap between the reflector plate and absorber. A numerical model was developed to determine the overall heat transfer coefficients for an East-west oriented CPC with a low concentration, incorporating non-

continuous tracking, at different angles of inclination. The results demonstrated a variation of 10% in the convective heat transfer coefficient with tilt angle.

Rönnelid and Karlsson (1996a) investigated the effect of geometrical arrangements and various material properties, including the thermal and optical properties of insulation, reflectors and absorbers, on the heat loss properties of CPCs with flat plate absorbers. The collector models with different geometric and material configurations were electrically heated in a 'hot box'. The recommendations concluded from the results include using low emissivity absorbers and thin, low emissivity reflectors, and applying a secondary glazing to the top of the collectors that is opaque to infrared light.

The effect of an air gap between the absorber and reflector on the overall heat loss coefficient was also investigated and found to be minimal. Although this study is limited by a maximum temperature difference of 75°C, the relationships between the properties evaluated and the heat transfer coefficient seem to be linear, and can thus be extrapolated for high temperature applications.

A second study by Rönnelid and Karlsson (1996b) involved comparing the performance of a 13.6 m^2 aperture area, flat-absorber CPC with a flat plate collector of the same area. Both collectors were fabricated and tested and had a Teflon glazing applied to the top. At a temperature of 70°C the heat loss properties of the collectors were described by an efficiency of $F'\eta_0 = 0.75$ and a heat loss coefficient of $F'U_L = 2.5$ $Wm^{-2}K^{-1}$ for the CPC and $F'\eta_0 = 0.80$ and $F'U_L = 3.3$ $Wm^{-2}K^{-1}$ for the flat plate collector. Simply put, the CPC-collector experiences less heat loss and the large differences were attributed to the absorption of solar radiation in its reflectors.

Yadav et al. (1996) fabricated a low-cost CPC with a tubular absorber from materials available locally in India. Despite using materials with poor thermal and optical properties, such as saw dust insulation and a galvanized iron reflector, a stagnation temperature of 92°C was achieved within two hours from the start time of 11:05.

Khalifa and Al-Mutawalli (1996) compared the thermal performance of a stationary CPC fixed at an optimal angle, and a two-axis electro-mechanical sun-tracking system. Both systems were designed and evaluated by varying the flow through the collectors. The tracking CPC performed better than the fixed collector, increasing collected energy by up to 75%.

A study by Adsten et al. (2005) focuses on an asymmetric truncated CPC, a development that maximizes solar yield at high latitudes, where the annual solar radiation is asymmetric. The design included a bi-facial absorber and various configurations were fabricated and tested. The collectors operated at a temperature of 75°C and could be used for concentrators for PV-modules. This type of collector is ideal for a country like Sweden, where the annual solar radiation varies significantly, as opposed to South Africa, where it does not.

Kim et al. (2007) compared the thermal performance of a stationary CPC with a North-South oriented, single-axis sun-tracking CPC. Evacuated tubes and electronic tracking was implemented in the designs and the CPCs were evaluated by comparing irradiation, flow rate and temperatures. The results obtained showed that the tracking CPC was more stable, with a 14.9% higher thermal efficiency than the stationary collector.

Tang and Yu (2010) investigated the feasibility and optical performance of CPC collector that is adjusted to three positions throughout the day, facing east, upward and west in turn, which is named a 3P-CPC. This CPC is used to concentrate light onto photo-voltaic cells and its performance is compared to a fixed East-West oriented CPC, or EW-CPC, with a half acceptance angle equal to that of the 3P-CPC. The 3P-CPC collected between 26% and 45% more energy than the fixed EW-CPC. A clear drawback of this design is the manual adjustment needed, the angles of which also change throughout the year.

A study by Tiba and Fraidenraich (2011) focused on non-evacuated, stationary CPCs with wedge receivers. CPCs with different low concentration ratios between 1 and 2 were analysed and the effect of the concentration ratio, tilt angle and reflector material reflectivity was evaluated and compared to a flat-plate collector. The simulation results indicated that for relatively low temperatures and concentration ratios, the CPCs performed better than the flat-plate collectors, with an increase in thermal energy collection of up to 55% when the reflectivity is increased to between 0.86 and 0.96. Furthermore, of fabrication of CPCs instead of FPCs would save around 60% of the absorbent material.

Su et al. (2012) did a comparative study between a normal mirror reflector profile CPC, a solid CPC made from a dielectric such as acrylic or polycarbonate, and a lens-walled CPC. The lens-walled CPC presented consists of a thin lens-shaped wall in the CPC profile with a mirrored coating on its back surface, with the refraction of the lens leading to a larger acceptance angle. All three CPCs had a concentration ratio of 2.5 and were analysed with PHOTOPIA to determine the optical efficiencies at different incident angles.

While the lens-walled CPC only achieved about 80% of the accumulative solar energy collection of the solid CPC, it performed 20-30% better than the mirrored CPC, showing itself to be a promising development.

Gudekar et al. (2012) presented a cost effective and easy to fabricate and operate CPC for steam generation applications. The collector requires a single daily tilt adjustment during its 6 hour operation time, and requires less mirror material than conventional CPC designs due to being truncated. The top portion of the reflector profile of a CPC contributes little to the collected energy, thus it is sometimes truncated to save on material costs and space. The thermal efficiency of the system was estimated at 71%.

Li et al. (2013) compared the performance of two CPC with concentration ratios of 6 and 3 respectively, which translates to a half acceptance angle of 3° and 10°. The CPCs contain U-shape evacuated tubes and do not have gap-losses. The thermal efficiencies for the 3x CPC reached up to 40% and 46% for the 6x CPC, at an operating temperature of 200°C. However, the 6x CPC requires five daily tilt adjustments, while the 3x CPC does not require any, only needing adjustments throughout the year.

A study by Kim et al. (2013) modelled, analysed, fabricated and tested two different stationary CPCs with a North-South orientation and East-West orientation respectively. The systems consists of evacuated counter-flow absorber tubes with external reflectors. The systems were shown to achieve efficiencies of more than 40% above 200°C, and also showed that an E-W orientation outperforms a North-South orientation.

Wang et al. (2015) developed a tracking compound parabolic concentrating (TCPC) solar collector with a concentration ratio of 2.3. The sun-tracking is electro-mechanical and involves using a crank rod transmission mechanism to rotate the North-South oriented CPCs. The system also included evacuated tubular receivers. While tracking, the average optical efficiency of the TCPC was more than 60%, compared to around 30% when fixed. The tracking mode also increases the energy output by 90-130%. Also programmed into the system is an intermittent tracking mode, the average optical efficiency of which is 3.6% higher than that of the continuous tracking mode.

2.2 Stationary CPCs used in solar-driven absorption systems

Tamainot-Telto and Critoph (1999) developed a CPC for an ammonia-carbon sorption refrigerator with a concentration ratio of 2.4 and half acceptance angle of 25°. With 500 W of solar input, the sorption refrigerator provided cooling power of up to 120 W at an ambient temperature of 20°C. The CPC was designed to replace the older flat collector present in an experimental solar sorption cooling unit of Critoph from 1994, in order to increase solar efficiency. Temperatures of up to 172°C were achieved and recommendations included applying double glazing or evacuation to achive higher temperatures.

Florides et al. (2002) modelled and simulated a domestic-sized absorption solar cooling system with the heat input provided by a 15 m² compound parabolic collector. The system comprised the CPC, storage tank, boiler and a LiBr-water absorption refrigerator and would provide 11 kW of cooling capacity, from a maximum heat input of 15 kW, determined by a TRNSYS simulation. This cooling capacity was determined sufficient to satisfy the cooling needs of a well-insulated domestic dwelling. In order to be economically competitive, the cost of the total system would have to be decrease by more than 60%, a possibility if mass produced. Furthermore, the CO_2 contribution of this system would be 20% less than a conventional R-22 air conditioner.

A study by Rivera and Rivera (2003) investigated the theoretical performance of an intermittent absorption refrigeration system making use of an ammonia-lithium nitrate mixture. A CPC acts as the generator for the system, with efficiencies varying between 0.33 and 0.78 depending on the time of day and season. With a generation temperature of around 120°C, the system would be able to produce up to 11.8kg of ice, with an overall system efficiency of between 0.15 and 0.4.

Ahgbalou et al. (2004) evaluated the performance of an absorption refrigerator that makes use of an activated carbon-pair ammonia, which is used for its ability to absorb a large amount of ammonia. In order to reduce the size of the system to make it economically viable, rapid cooling and heating is needed. Therefore, a detailed model was developed that computes temperature and absorbed mass for a given heat flux, leading to a simulation of the system with compound parabolic concentrating heat pipes inserted into the generator. A nominal solar coefficient of performance (COP) of 14.37% was achieved, though the effect of cloud coverage and other detrimental weather effects on the COP was not discussed.

In a study by Lambert (2006), a solar powered absorption heat pump used for residential heating and cooling was designed, modelled and analysed. The system utilizes an ice thermal storage reservoir, which provides 24h cooling, and a heat pump that uses a carbon-ammonia absorbent refrigerant pair. In order to achieve the operating temperature of 170°C, the solar collector types deemed satisfactory are either a CPC with a concentration ratio of 10 or more, or a flat plate collector with evacuated tubes. The estimated COP of this system is 1.6, compared to the highest previously reported experimental value of 1.2 by Tchernev in 1989.

Ortega et al. (2007) developed a numerical model to describe the heat and fluid dynamic behaviour inside a CPC used as a vapour generator for an ammonia absorption cooling system. The analysis focused on increasing ammonia-water vapour production, by varying the properties of the CPC, such as reflectivity and half acceptance angle, while using a 35m long CPC. The results showed that at a solar efficiency of 46.3%, the system could produce 3.8kW of cooling at -10°C.

Moodaly (2008) developed a model to determine solar radiation and the most efficient orientation of a CPC for use in an aqua-ammonia absorption refrigeration system. It was concluded that an East-West orientation provides the best performance. In the experimental setup, a small-scale CPC with a concentration ratio of 1.74 achieved a peak stagnation temperature of 138°C.

Continuing the study by Rivera and Rivera (2003), Rivera et al. (2010) evaluated the actual performance of the solar intermittent refrigeration system using ammonia/lithium nitrate for ice production presented in the 2003 study. A nominal capacity of 8kg of ice per day was achieved with evaporator temperatures as low as -11°C. The solar coefficient of performance peaked at 0.08 and it was found that the solar COP increases with an increase of solar radiation.

A study by Lu et al. (2013) incorporated medium evacuated tube CPC solar collectors into a two-phase thermos-syphon silica gel-water solar adsorption chiller and a $LiBr-H_2O$ absorption chiller in Dezhou City, China, and Jinan City, China, respectively. The results showed that the first system achieved an average solar COP of 0.16 and could provide 15°C chilled water for 7½ hours with a hot water temperature of 125°C, while the second system achieved an average solar COP of 0.19 and could provide chilled water for only 4½ hours.

In a more recent study by Winston et al. (2013), the inventor of the CPC and his colleagues developed, fabricated and operated a 23kW double effect LiBr absorption chiller for two cooling seasons in 2011 and 2012. The chiller is powered by 53.3m^2 of stationary CPC collectors with external reflector profiles. Both systems were analysed in both sunny and cloudy conditions, with the collectors maintaining average temperatures of 160-200°C. While in this range, the CPCs achieved an average efficiency of 36.7% with peak efficiency at 40%. The thermal COP of the entire system averaged at 0.99, while the solar COP averaged at 0.363. The simplicity of the CPCs make them highly attractive and economically feasible for cooling projects and are currently being commercialized in India and the U.S.

2.3   Sun-tracking mechanisms

Sun-tracking with regards to solar collectors has been done in various ways. In some studies, two-axis tracking was implemented, with the collector being a flat plate or dish. This would be unsuitable for a CPC as it only has one axis on which to rotate. Other studies have collectors which angle must be manually adjusted every few hours.

While this would be a suitable method of tracking, for the purpose of this study, the complete system must be able to be left alone for hours or days at a time, which makes this method less than ideal. The most suitable method of sun-tracking for a CPC involve single-axis tracking, though no study has yet applied tracking CPCs to aqua-ammonia absorption refrigeration systems.

Farouk Kothdiwala et al. (1995) experimented with an ETC with an external CPC profile that incorporated continuous tracking. Though the specific method of tracking is not mentioned, it is noted that the results demonstrated a variation of 10% in the convective heat transfer coefficient with tilt angle. Manual adjustment of the inclination angle is also investigated, with as little as 12 adjustments annually, with favourable results.

Khalifa and Al-Mutawalli (1996) incorporated a two-axis electro mechanical sun-tracking system in a CPC system and compared it to the performance of a stationary CPC at an optimal angle. The tracking system functioned by ensuring that two photo-transistors receive the same amount of solar radiation, i.e. when they are normal to the sun's rays.

When they receive inequal amount, a voltage-difference amplifier activates a gearbox and DC motor that steers the collector around the desired axis until the voltage difference is eliminated. This process happens every 3 to 4 minutes horizontally and 4 to 5 minutes vertically, allowing the collector to move the equivalent of one degree. It was found that by using a tracking CPC, the energy gain increased by up to 75%.

Kim et al. (2007) constructed a stationary CPC and North-South facing CPC with single-axis sun-tracking and compared the results of the two. The tracking was done mechanically with servos on three concentrators and it was found that the results of the tracking CPC resulted in a 14.9% higher thermal efficiency than the stationary collector. The tracking CPC fared especially well in the early morning and late afternoon in comparison with the stationary CPC.

Tang and Yu (2010) experimented with a CPC collector that could be manually adjusted during the day to three different positions. They also constructed a stationary CPC for comparison. The angles consisted of 45° toward the morning sun eastward, 0° with the ground at midday, and 45° toward the afternoon sun westward. The position of the collector was manually adjusted and locked into place. The results showed that the adjustable CPC absorbed between 26% and 45% more heat annually than the stationary CPC.

In a recent study by Wang et al. (2015) a tracking compound parabolic concentrating collector was developed that utilised an electro-mechanical sun-tracking system. The system worked by connecting crank rods to each collector, all connected to a single bar which was driven by an electric motor. This translated the lateral motion into rotational motion, allowing the collectors to be set up to rotate through different angles.

It is unclear whether the working of the electric motor was controlled by a computer program or manually controlled, though the former seems more likely and alluded to. Wang also ensured that enough space exists between each concentrator that occlusion between them will not occur. Comparing the results from the CPC when stationary to when it was tracking showed that the energy output was increased by between 90% and 130%, with 60% more optical efficiency.
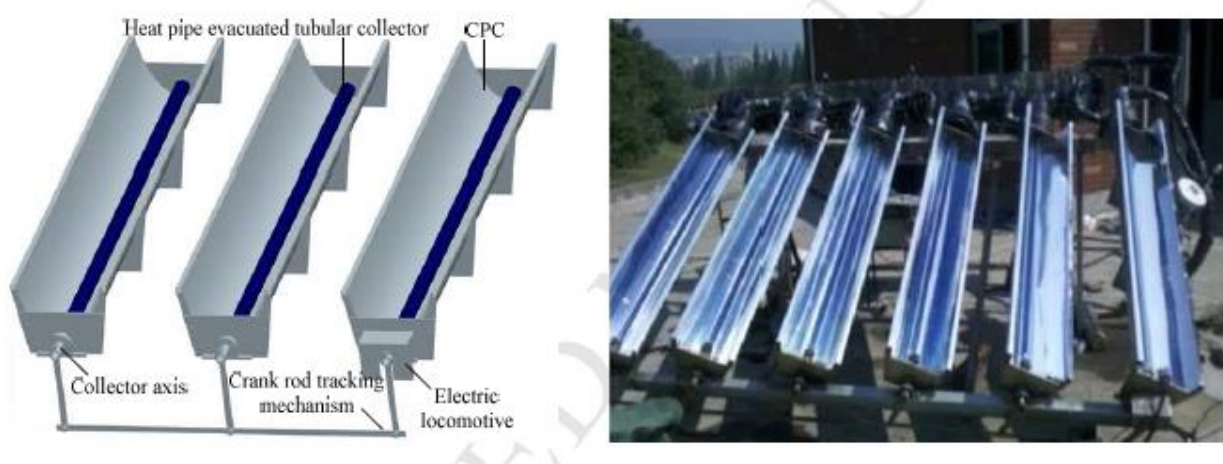

Figure 9: Crank rod sun-tracking mechanism used by Wang et al. (2015)

2.4 Summary

From the literature it is clear that concentrating parabolic collectors are the most suitable for the purposes of this study. They are able to deliver high temperatures, can be manufactured fairly easily and result in a much lower heat loss. The costs vary depending on the coatings and features in the design, but a relatively low-cost CPC can be designed if evacuated tubes and silver coatings are disregarded. These features are more useful when much higher temperatures are required.

Flat plate collectors (FPCs) were not considered for this study due to their relatively low resulting temperature and high heat loss. While the output temperature can be increased, doing so usually requires applying expensive coatings or using evacuated tubes, which are fragile and expensive.

Parabolic trough collectors (PTCs) were not considered due to the fact that they require very precise sun-tracking. While such a system would be possible to construct and suitable for the purpose of the study, it would require expensive and delicate equipment, which could be damaged during the course of the other concurrent studies. Even if a component on a tracking CPC is damaged, the concentrators could be locked at a certain optimal angle and function well while repairs are made, while a PTC would be out of commission until repairs are complete.

A similar sun-tracking system to that of the study by Wang et al. (2015) would increase the optical efficiency of the CPC as well as the amount of heat that can be absorbed. However, the decision was made to make as little use as possible of electricity and electronics in the design of the collector, as the full system may be tested in a remote location. A crank rod mechanism could still be used by exchanging the electric motor for a weight-driven, pendulum-timed clockwork system, similar to those used in tower clocks. The working of this tracking system will be described in Chapter 5.2.

3 Theory

The following chapter describes the theory applicable to this study and is based on the theory as presented by Winston et al. (2005) and Kalogirou (2009).

3.1 Solar Angles

In order to determine the sun's motion relative to an observer, it is useful to consider the earth as fixed and to describe the sun's virtual motion in the sky by using a fixed coordinate system with its origin at the location of the observer. As shown in Figure 10, this motion can be accurately defined by constraining the sun's movement with 2 degrees of freedom on a sphere, thus its position with respect to an observer can be described by two angles, the solar altitude (α), and the solar azimuth (z). In order to determine these angles, the solar declination and hour angle need to be calculated.

The solar declination (δ) is a description of the angular distance of the sun's rays north or south of the equator, with a positive declination indicating rays north of the equator. This angle varies throughout the year as the earth revolves around the sun, as shown in Figure 11, a maximum of 23.45° occurring on the winter solstice and summer solstice and a 0° declination on the equinoxes.

The declination, in degrees, for any day of the year can be approximated by the following equation:

$$\delta = 23.45 \, sin\left[\frac{360}{365}\,(284 + N)\right] \tag{3.1.1}$$

where N is the day of the year.

The hour angle, h, is the angle through which the earth would have to turn to bring the meridian of a point or the earth's surface directly under the sun. The hour angle at solar noon would be zero, with 15° equivalent to 1h, and afternoon hours designated as positive.

The hour angle in degrees can be expressed as:

$$h = \pm 0.25 \, (Number \; of \; minutes \; from \; local \; solar \; noon) \tag{3.1.2}$$

where the plus sign applies to afternoon hours, and the minus sign to morning hours.
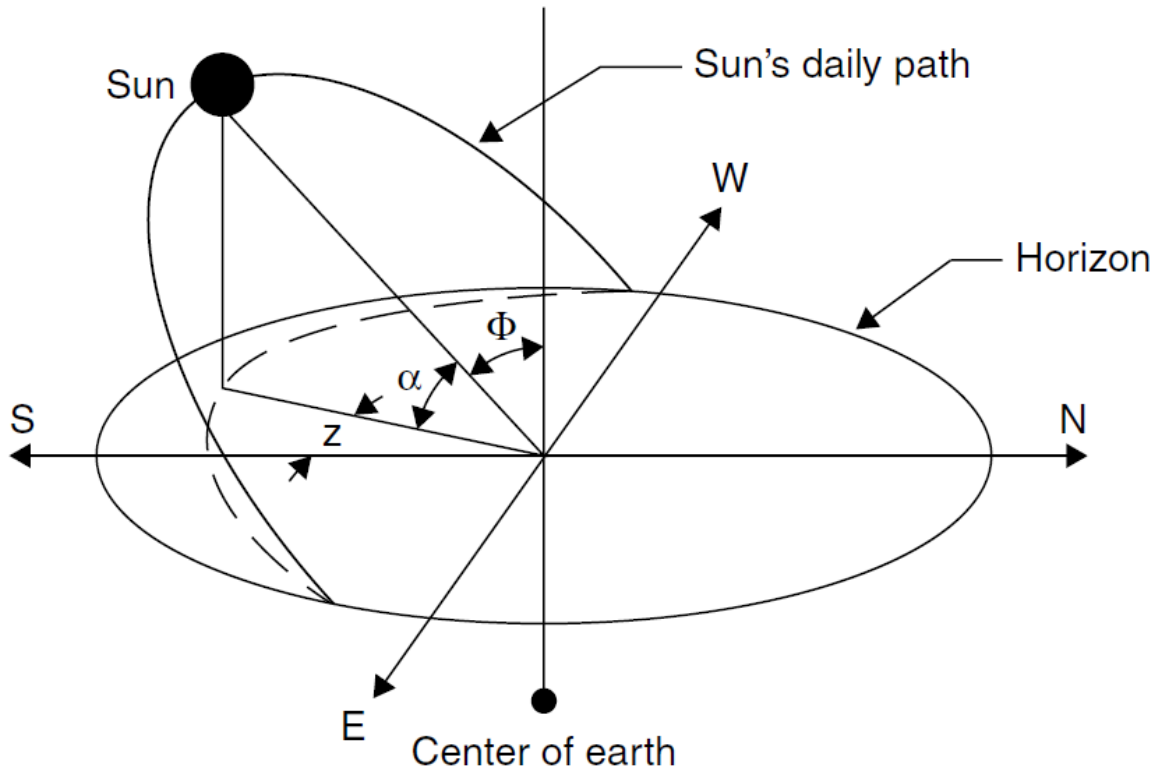
Figure 10: Apparent daily path of the sun across the sky relative to an observer (Kalogirou, 2009:58)
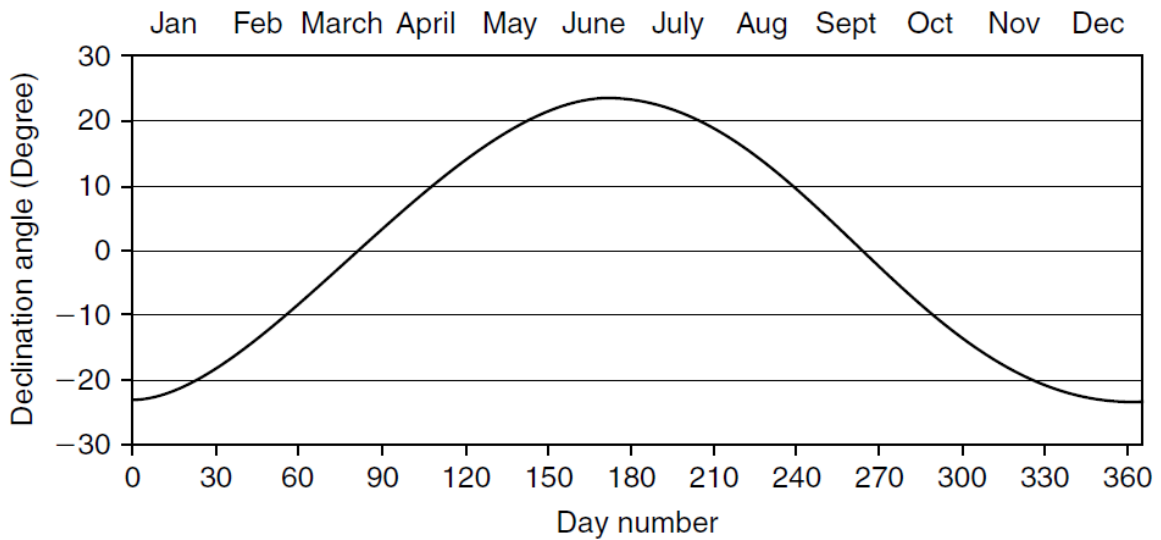

Figure 11: Declination of the sun throughout the year (Kalogirou, 2009:55)

The solar altitude angle, α, describes the angles between the horizontal plane and the sun's rays, and can be expressed by the following equation:

$$\sin(\alpha) = \sin(L_{at})\sin(\delta) + \cos(L_{at})\cos(\delta)\cos(h) \qquad (3.1.3)$$

where L_{at} is equal to the local latitude of the site of interest.

The solar azimuth angle, *z*, describes the angle of the sun's rays in the horizontal plane from due north in the Southern Hemisphere, or due south in the Northern Hemisphere, with Westward being designated as positive. The angle is expressed by the following equation:

$$\sin(z) = \frac{\cos(\delta)\sin(h)}{\cos(\alpha)} \qquad (3.1.4)$$

3.2 Compound parabolic concentrator optics

The law of reflection states that, when light is reflected, the angles that the incident and reflected rays make with the normal of the surface, is equal and lie in the same plane. The following equation shows this relationship:

$$cos\Theta_i = cos\Theta_r \qquad (3.2.1)$$

where Θ_i and Θ_t is the indicent angle and reflected angle, respectively.

When light is transmitted to another medium, Snell's law of refraction states that ratio between the sine of the angle between the normal and incident ray, and the sine of the angle between the normal and refracted ray, is constant, as illustrated by Figure 12 and the following equation:

$$n_i sin\Theta_i = n_t sin\Theta_t \qquad (3.2.2)$$

where n_i and n_t are the indices of refraction for the two media.

In order to design a profile for a compound parabolic concentrator, a method known as 'ray tracing' is employed, forming a profile by following the path of light rays through a system of reflecting and refracting surfaces.
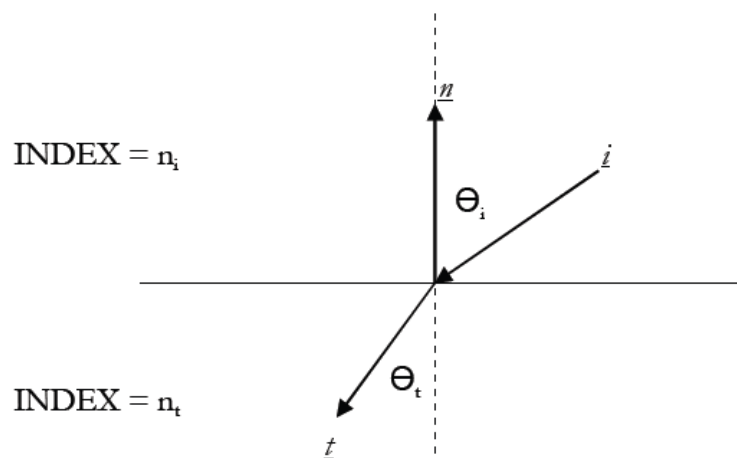

Figure 12: Diagram illustrating the unit vectors for Snell's law of refraction

The profile of a 2D CPC has the equation:

$$C = \frac{n_d}{sin\Theta_a} \qquad (3.2.3)$$

where C is the concentration of the CPC, n_d is the refractive index of the medium though which light is travelling and Θ_a is the acceptance angle. The acceptance angle of a CPC describes the angle of which the edges of the angle is the limit through which light can enter and still hit the absorber.

To manually trace the CPC profile, 'ray tracing' is performed, while adhering to Fermat's principle, which states that the optical path length of all rays between the object and image remains the same. This is done by viewing the light rays as 'strings' with a fixed length, connected perpendicularly to a slider on a rod at an angle to the aperture entrance equal to the acceptance angle, as shown in Figure 13.

The string is fixed at point D, follows the absorber through B', connects to point A and ends at point C. The slider is then moved down the rod, keeping the string length constant, and the path described by the movement of point A is the CPC profile.
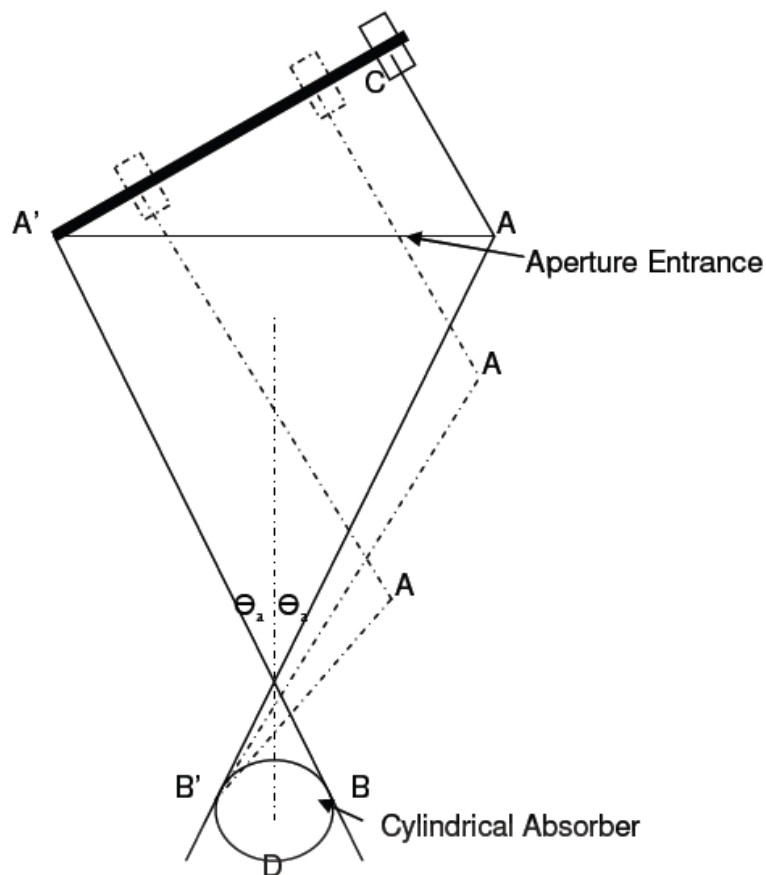

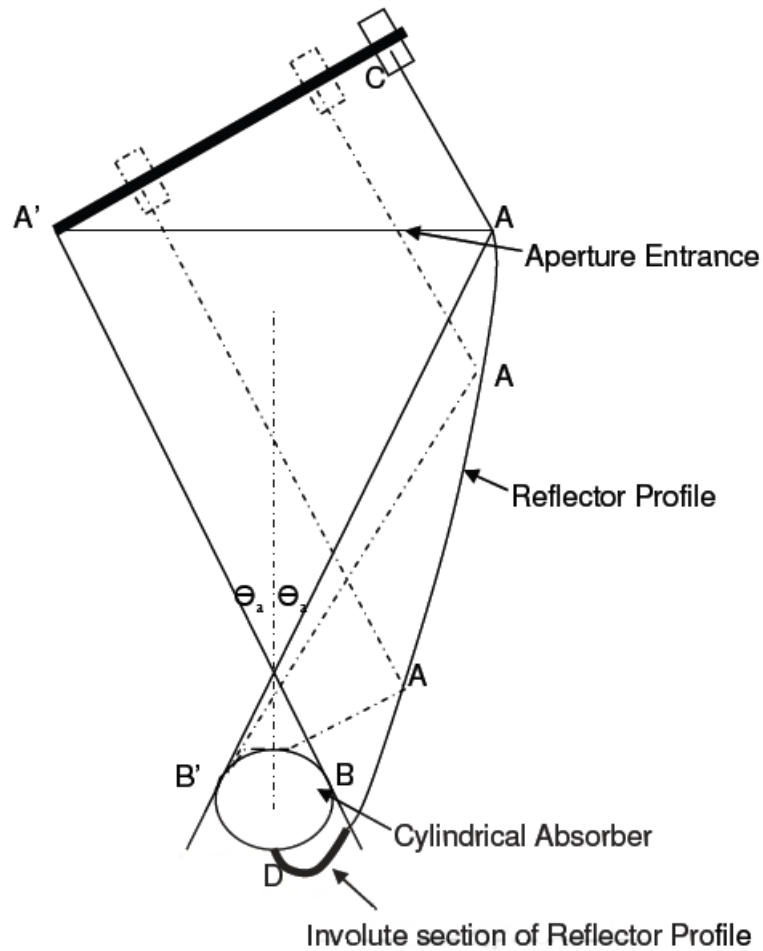**Figure 13: Diagram illustrating the tracing of a CPC profile**

Figure 14: Diagram illustrating the involute of a CPC profile

For the reflector profile below the absorber, an involute of the cylinder is created, starting at point D, as shown in Figure 14. The involute shape is made by tautly unwinding a string wrapped around the cylinder back from point D until it reaches the rest of the traced profile.

Developing a profile by the using 'ray-tracing' method requires manual adjustments and tracing and it time intensive. A more efficient method of creating the profile is to define it with equations.

The aperture entrance of the CPC is defined by:

$$a = \frac{a'}{sin\Theta_a} \qquad (3.2.4)$$

where a' is the absorber size. This implies that:

$$\frac{a}{a'} = \frac{1}{sin\Theta_a} \quad or \quad C = \frac{a}{a'} = \frac{1}{sin\Theta_a} \qquad (3.2.5)$$

The overall length of the CPC is expressed by the following equation:

$$L = \frac{a'(1+sin\Theta_a)cos\Theta_a}{sin^2\Theta_a} \quad or \quad L = (a + a')cot\Theta_a \qquad (3.2.6)$$

For a flat absorber CPC, as shown in Figure 15, and for different values of Φ, the following equations are applicable for the coordinates of point R:

$$y = \frac{[2a'(1+sin\Theta_a)\sin(\Phi-\Theta_a)]}{[1-cos\Phi]} - a' \qquad (3.2.7)$$

and $$Z = \frac{[2a'(1+sin\Theta_a)\cos(\Phi-\Theta_a)]}{[1-cos\Phi]} \qquad (3.2.8)$$

For a CPC with a tubular absorber, such as shown in Figure 16, a distance t is defined as the distance between point R on the profile and the corresponding tangent point on the absorber for any value of Θ. This distance t is expressed by:

$$t = \frac{r\left[\Theta+\Theta_a+\frac{\pi}{2}-\cos(\Theta-\Theta_a)\right]}{[1+\sin(\Theta-\Theta_a]} \quad for \quad \frac{\pi}{2} + \Theta_a < \Theta < \frac{3\pi}{2} - \Theta_a \qquad (3.2.9)$$

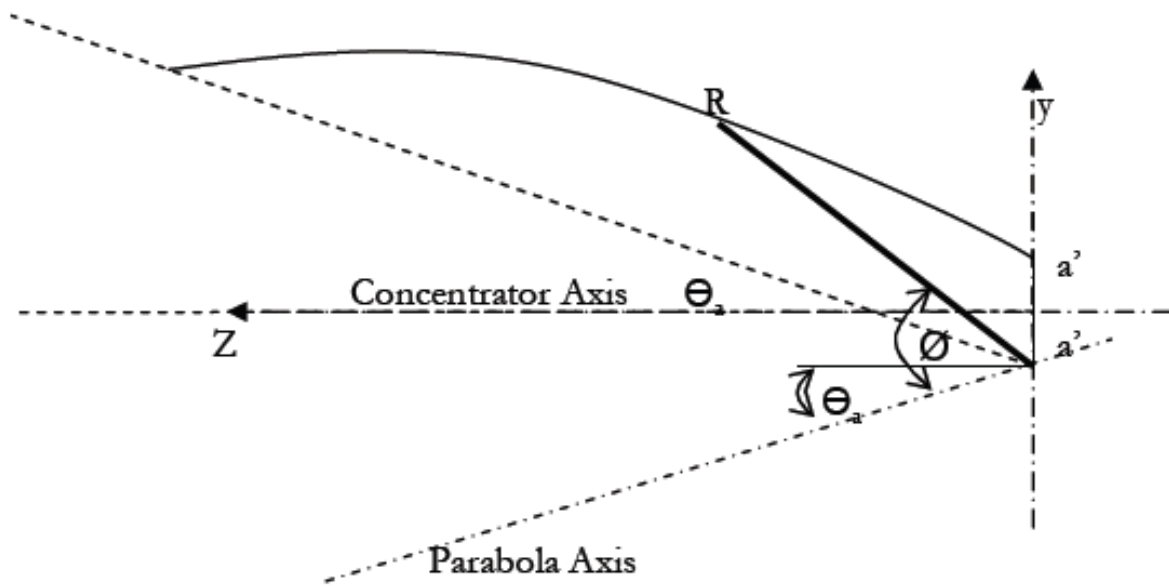and (for the involute section) $$t = r\Theta \quad for \quad \Theta < \frac{\pi}{2} + \Theta_a \qquad (3.2.10)$$

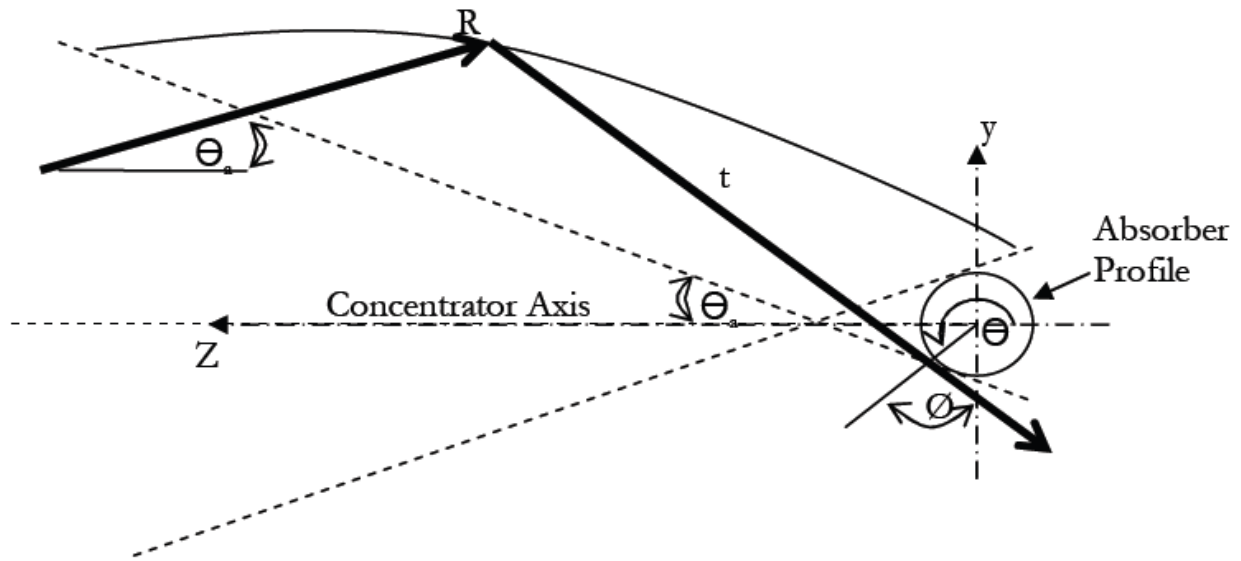Figure 15: Variables in CPC design for a flat absorber

Figure 16: Variables in CPC design for a tubular absorber

3.3 Thermal analysis of compound parabolic collectors

The instantaneous efficiency, η, of a CPC is defined by the following equation:

$$\eta = \frac{Q_u}{A_a G_t} \tag{3.3.1}$$

where G_t is the total incident radiation on the aperture area, known as A_a.

Q_u is known as the useful energy gain, given by the following equation:

$$Q_u = F_R[SA_a - A_r U_L (T_i - T_a)] \tag{3.3.2}$$

where A_r is the area of the receiver or absorber.

The heat removal factor, F_R, indicates the ratio useable energy gain if the absorber was at the local fluid temperature, and can be calculated as:

$$F_R = \frac{\dot{m} c_p}{A_a U_L} \left(1 - exp \left[- \frac{U_L F' A_a}{\dot{m} c_p} \right] \right) \tag{3.3.3}$$

where $\dot{m}_{dot}$ is the mass flow and c_p is the specific heat of the fluid.

The collector efficiency factor is given by the equation:

$$F' = \frac{\frac{1}{U_L}}{\frac{1}{U_L}+\frac{D_O}{h_f D_i}+\frac{D_o}{2k}\ln\left(\frac{D_o}{D_i}\right)}$$

(3.3.4)

where D_o and D_i is the outer and inner diameter of the absorber, respectively, h_f is the convective heat transfer coefficient and k is the thermal conductivity of the pipe.

To calculate hf:

$$h_f = \frac{N_u k_f}{D_i}$$

(3.3.5)

where k_f is the thermal conductivity of the fluid and N_u is the Nusselt number of fluid with a laminar flow.

The overall heat loss coefficient, U_L, for a CPC has been determined by Hsieh (1983) as a factor of temperature and can be calculated by the following equation:

$$U_L = (0.18 + 16.95\varepsilon_r)[0.212 + 0.00255T_a + (0.00186 + 0.000012T_a)\left(\frac{T_o-T_i}{2} - T_a\right)$$

(3.3.6)

where T_a, T_i and T_o is the ambient, inlet and outlet temperatures, respectively, and ε_r is the emissivity of the receiver.

The absorbed solar radiation, S, is given as:

$$S = G_t \tau_{cover} \tau_{CPC} \alpha_r \gamma$$

(3.3.7)

where τ_{cover} is the transmissivity of the collector cover, α_r is the absorptivity of the receiver and τ_{CPC} is the effective transmissivity, defined by:

$$\tau_{CPC} = \rho^n$$

(3.3.8)

where ρ is the mirror reflectivity and n is the average number of reflections.

The correction factor for diffuse radiation, γ, is defined by the following equation:

$$\gamma = 1 - \left(1 - \frac{1}{C}\right)\frac{G_D}{G_t}$$

(3.3.9)

where G_D is the diffuse radiation.

The outlet temperature can also be calculated from the following equation:

$$T_o = \frac{Q_u}{\dot{m}c_p} + T_i$$

(3.3.10)

4 Mathematical Model

This chapter describes the mathematical model that was used to calculate the theoretical results of this study. All calculations are done with the location of Potchefstroom, South Africa, in mind.

4.1 Describing the sun-path

The local coordinates of Potchefstroom are 26°42'53" South and 27°06'10" East, giving a local latitude angle L_{at} of -26.715°.

By using equation (3.1.1) the solar declination angle, δ, can be calculated for each day of the year. Using equation (3.1.2) to equation (3.1.4), the hour angle, h, solar altitude angle, α, and solar azimuth angle, z, can be calculated for every 15 minutes of each day.

The solar altitude angle can be used to determine the angle at which the sun's rays will hit the reflector, by calculating an average altitude angle for each month. As shown in Figure 17, α varies from 86° in the summer to 41° in the winter. These values can be used to procure solar radiation data.

The solar azimuth angle is useful to determine the amount of time an East-West oriented CPC would be exposed to the sun's rays. The reflector would only be exposed to the sun when -90° < z < 90°. If the sun at any time moved behind the East-West line that can be seen in Figure 10, i.e. z < -90° or z > 90°, the reflector would not be exposed to the sun's rays, and thus would not be able to absorb solar radiation. For the purpose of this study, this amount of time was capped to 14 hours, in order to simplify the equations.

Furthermore, the amount of daylight hours need to be considered when determining the hours of exposure to the sun. Daylight hours can be defined as the amount of time for which the solar altitude angle is greater than zero, i.e. α > 0°. Figure 18 shows that at a certain point during the year, the amount of daylight hours become less than the amount of time the sun is not behind the East-West plane, with the interception points indicating when the equinoxes take place.

Correlating the two approaches, the average hours of exposure to the sun can be calculated for each month by determining the minimum of the two, as shown in Figure 19.
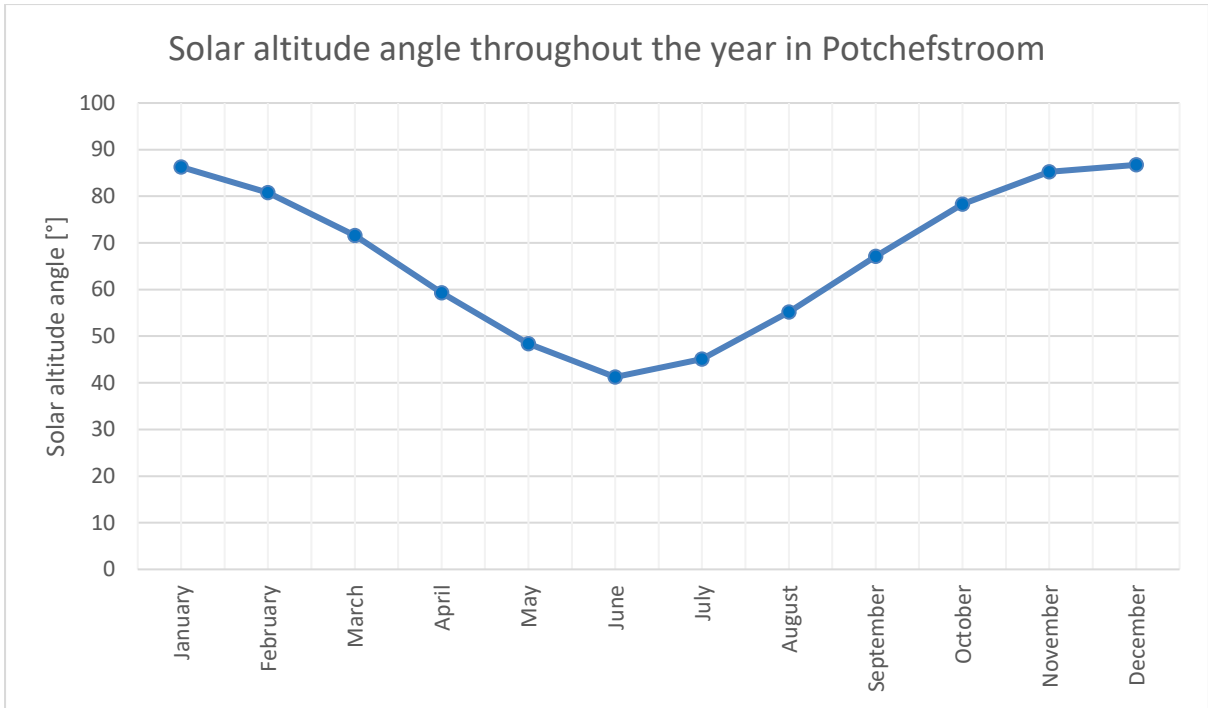
Figure 17: Graph showing the solar altitude angle throughout a year in Potchefstroom
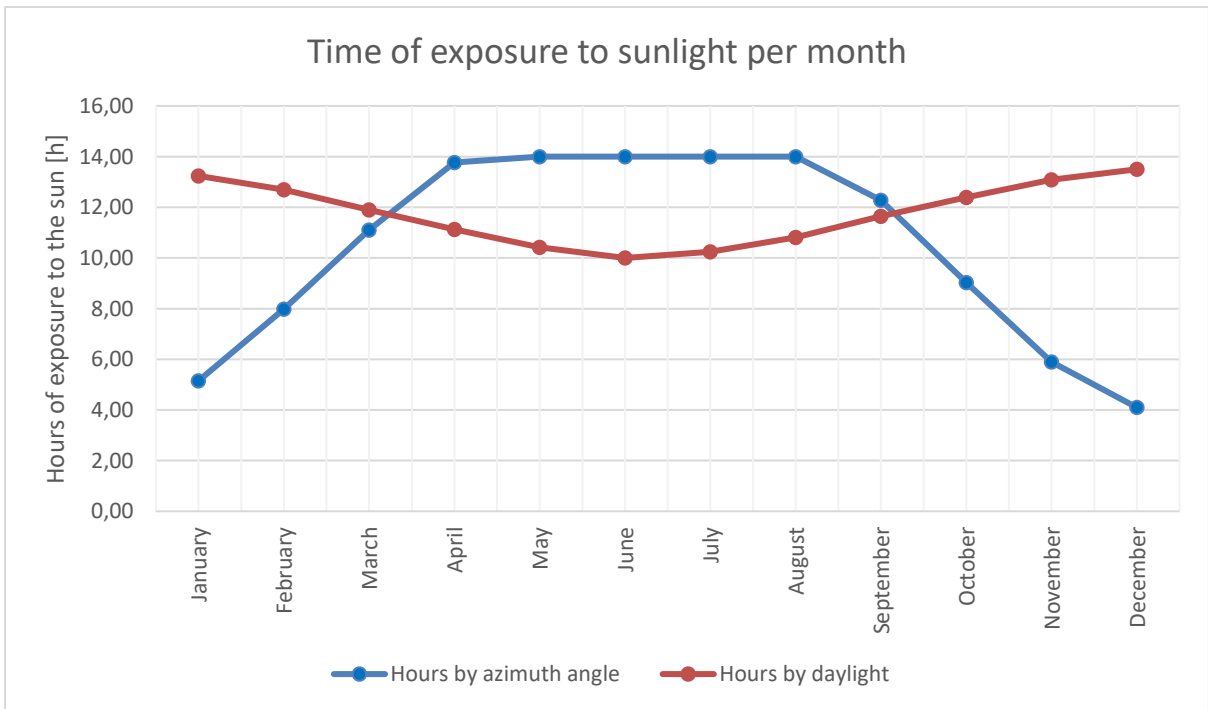

Figure 18: Graph showing time of exposure to sunlight by two different approaches
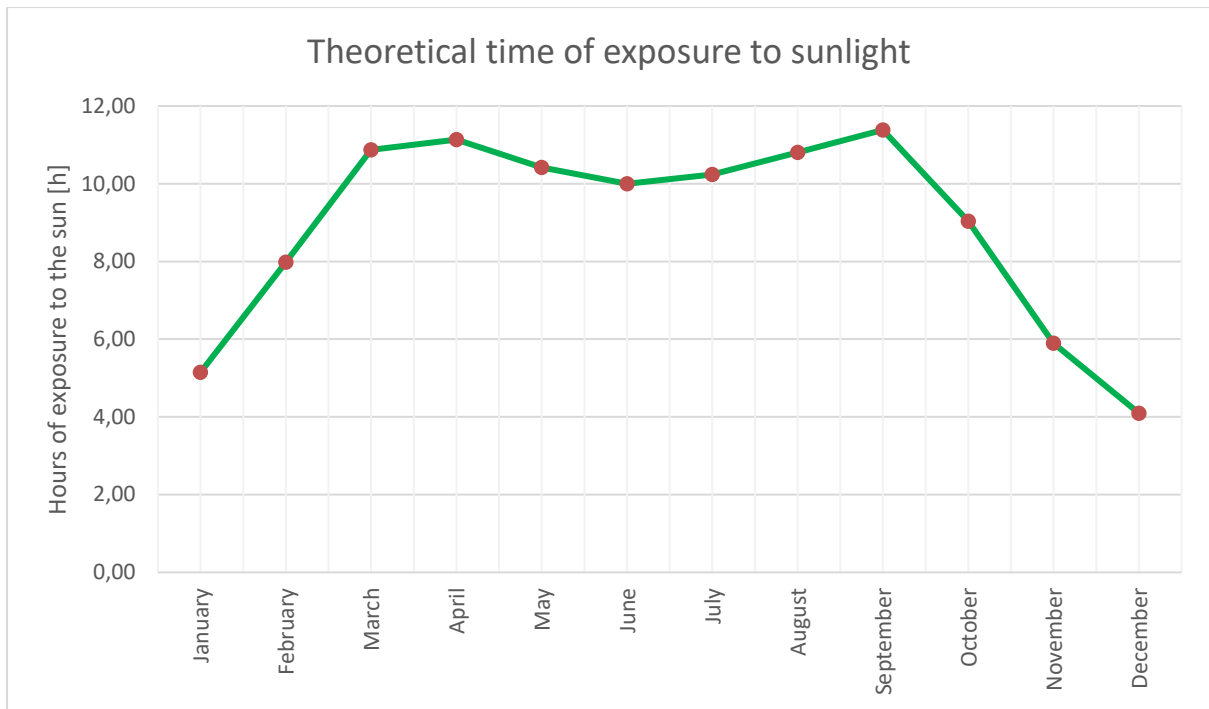
Figure 19: Graph showing the theoretical time of exposure to sunlight in Potchefstroom

4.2 CPC profile

To form the CPC profile, equation (3.2.4) to equation (3.2.10) was used and, in case of the coordinates, adapted to fit a vertical profile. Different combinations of receiver radius, r, and acceptance angle, Θ_a, were investigated in order to optimize the available space.

A CPC with a tubular receiver with a radius of 16 mm and an acceptance angle of 56° (half-acceptance angle of 28°), produces a profile with a concentration ratio, C, of 2.13, and a height, L, of 258.95 mm. The aperture size, a, would be 106.4 mm, with the aperture area, A_{CPC}, at 0.3575 mm^2. Figure 20 shows the designed CPC profile with a tubular receiver.

At a length of 1680 mm per CPC, 28 of these concentrators will be able to fit into the available space. This results in a total aperture area, A_a, of approximately 10 m^2.

However, the top portions of the reflector would not contribute much to the absorbed radiation, and thus the CPC is truncated by 22.77%. This results in new characteristic values for the CPC collector, which is summed up in Table 1.
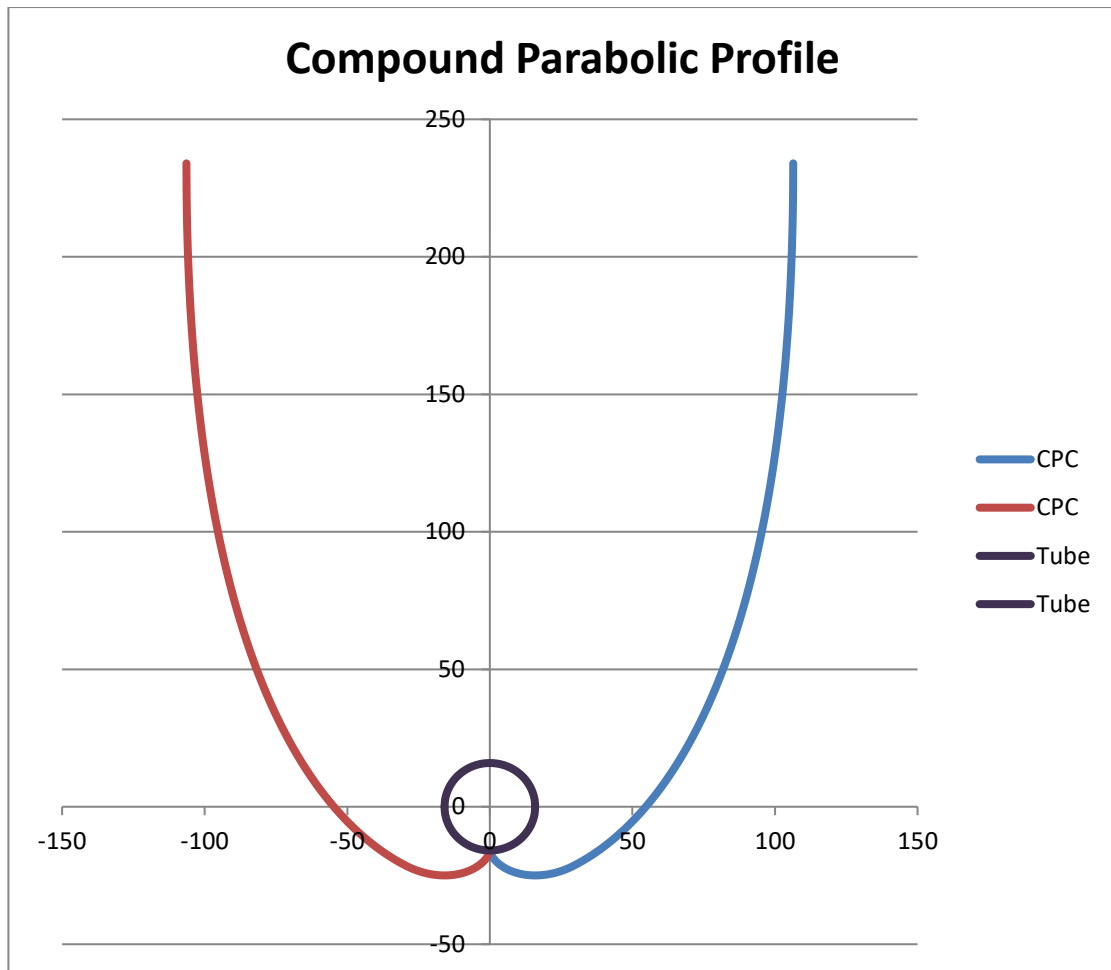
Figure 20: Profile of the designed CPC

Table 1: Characteristic values of the designed CPC

Properties	Symbol	Value	Unit
Concentration ratio	C	2.09	-
Receiver radius	r	16	mm
Acceptance angle	Θ_a	56	°
Half acceptance angle	$\Theta_a/2$	28	°
Aperture size	a	104.54	mm
Aperture area	A_{CPC}	0.3513	m^2
Total aperture area	A_a	9.84	m^2

4.3   Tracking the sun

In order to determine acceptable angles through which the collectors should rotate to still absorb radiation efficiently, tracking angle limits must be determined. The CPCs only need to rotate in such a way that the rays from the sun at the horizon and rays from sun at the midday solar altitude angle in summer, as well as winter, is within the acceptance angle of the CPC profile.

Thus, with a half acceptance angle of 28°, a summer altitude of 87° and a winter altitude of 41°, the normal of the CPC profile only needs to rotate from 10° with the horizon to 60°. This can be achieved through a rotating wheel and crankshaft mechanism.

With this rotation, all possible altitudes of the sun is included in the acceptance angle, and would allow the receiver to absorb radiation. This rotation start at 06:00 in the morning and end at 18:00 at night, rotating through the night from 18:00 to 06:00 the next morning as well. This is illustrated by Figure 21.

Figure 22 and Figure 23 compares the average solar altitude angles with the tracking acceptance limits for January and July, respectively. It is clear from these figures that allowing the normal of the CPC profile to vary between 10° and 60° will include all solar altitude angles and allow radiation to be absorbed at all times within the exposure time.

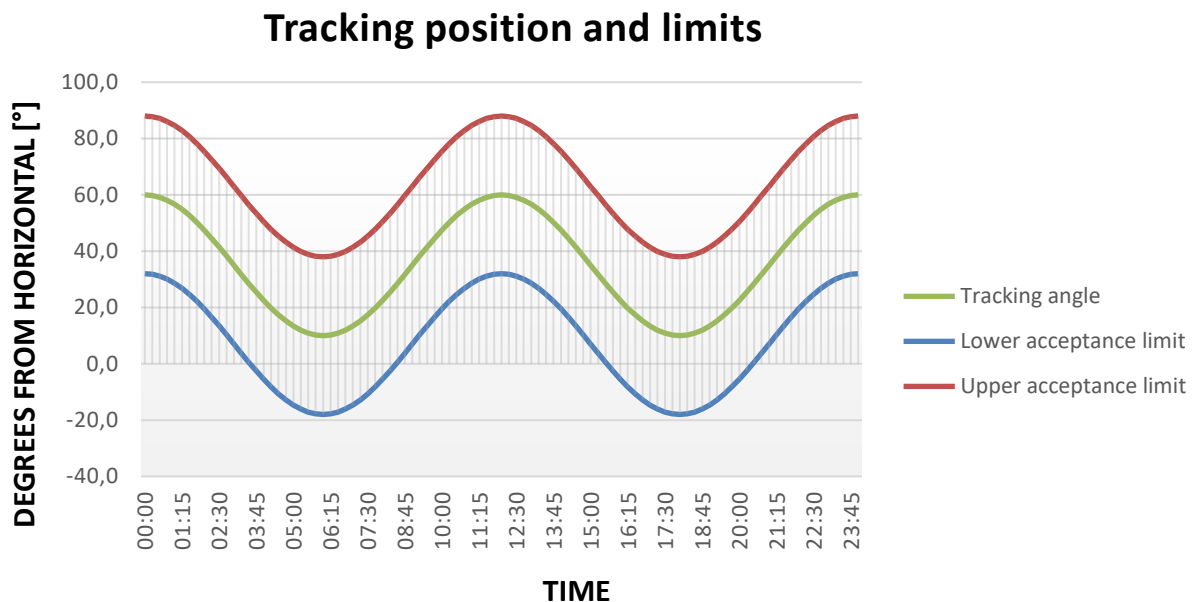
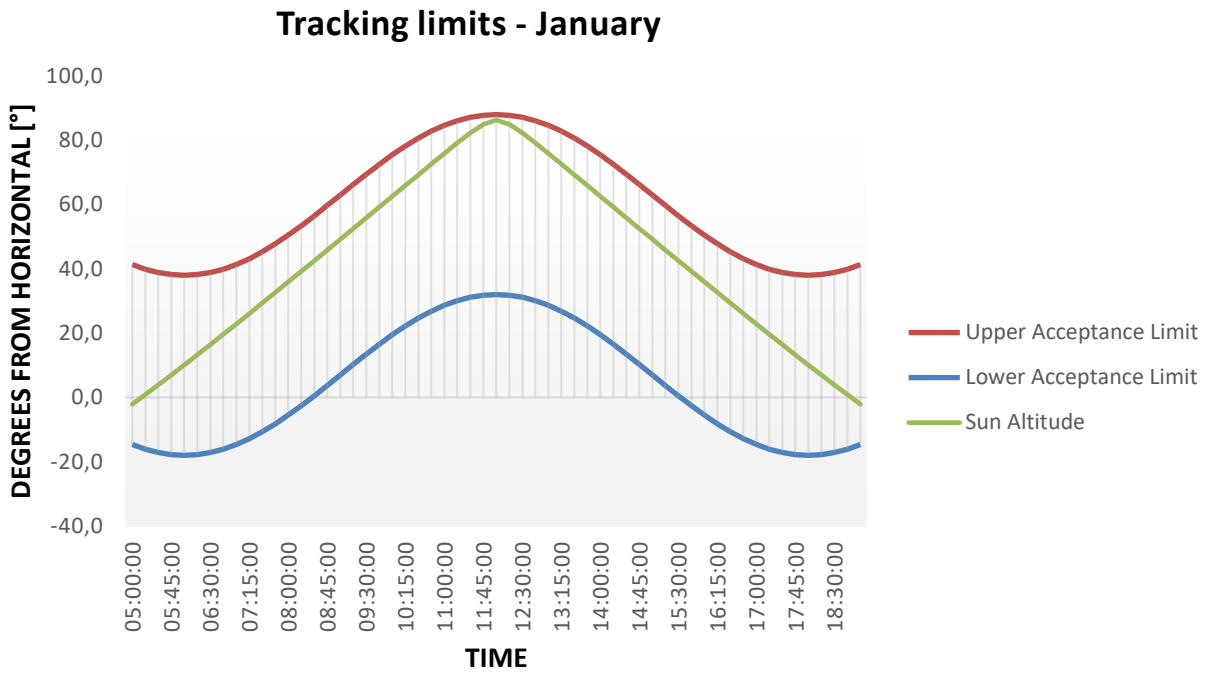**Figure 21: Graph showing the tracking angle and acceptance limits**

Figure 22: Graph showing the solar altitude angle and acceptance limits for January
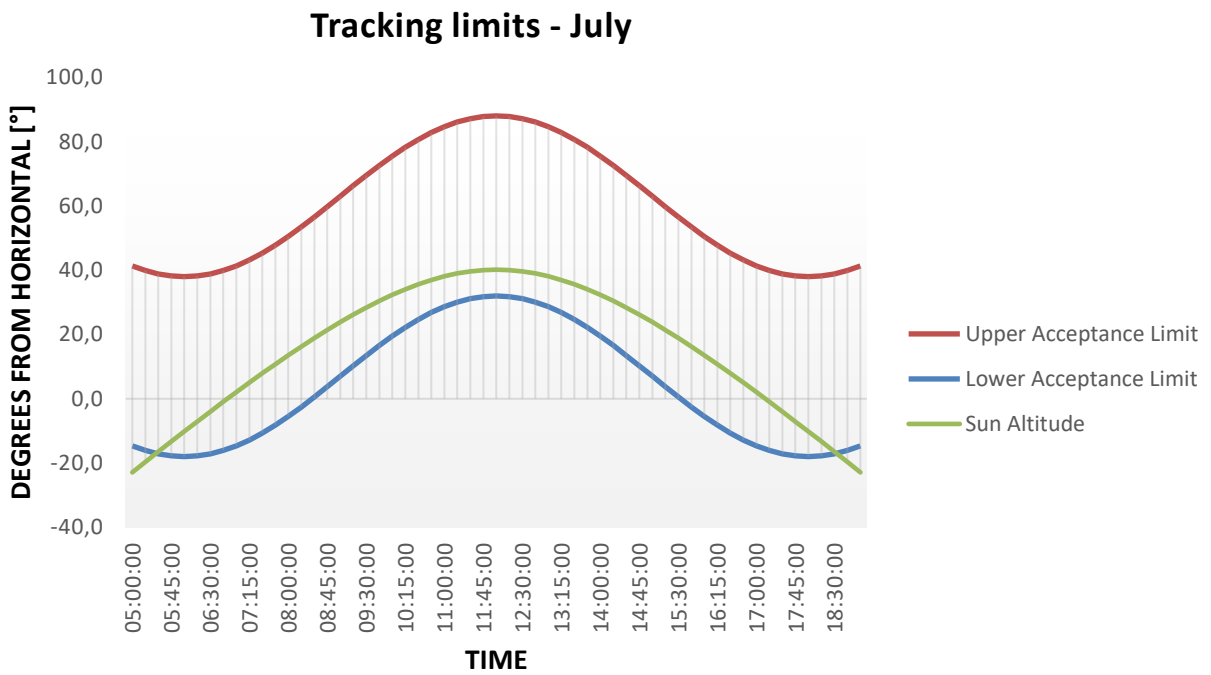

Figure 23: Graph showing the solar altitude angle and acceptance limits for July

4.4 Solar radiation data

A source for reliable solar radiation was found while studying a paper by Huld et al. (2012). The Photovoltaic Geographical Information System (PVGIS) is a web application that is widely used in Europe for the estimation of the performance of PV systems in Europe and, more recently, Africa, as shown in Figure 24.

In this application, solar radiation values in intervals of 15 minutes for each month can be obtained for anywhere within the available coordinates, including Europe, Africa and parts of Asia. If a surface tilt angle is entered, the output is adjusted accordingly, eliminating the need for lengthy equations. The application outputs include Global Irradiance, Diffuse Irradiance and Global Clear-sky Irradiance, all in W/m^2.

Using the tracking angle throughout the day as the tilt angle input, the three irradiance values can be obtained that takes into account the angle of the CPC aperture for every 15 minutes of a day, with unique average data for each month. Examples of these results for January and July are shown in Figure 25 and Figure 26.
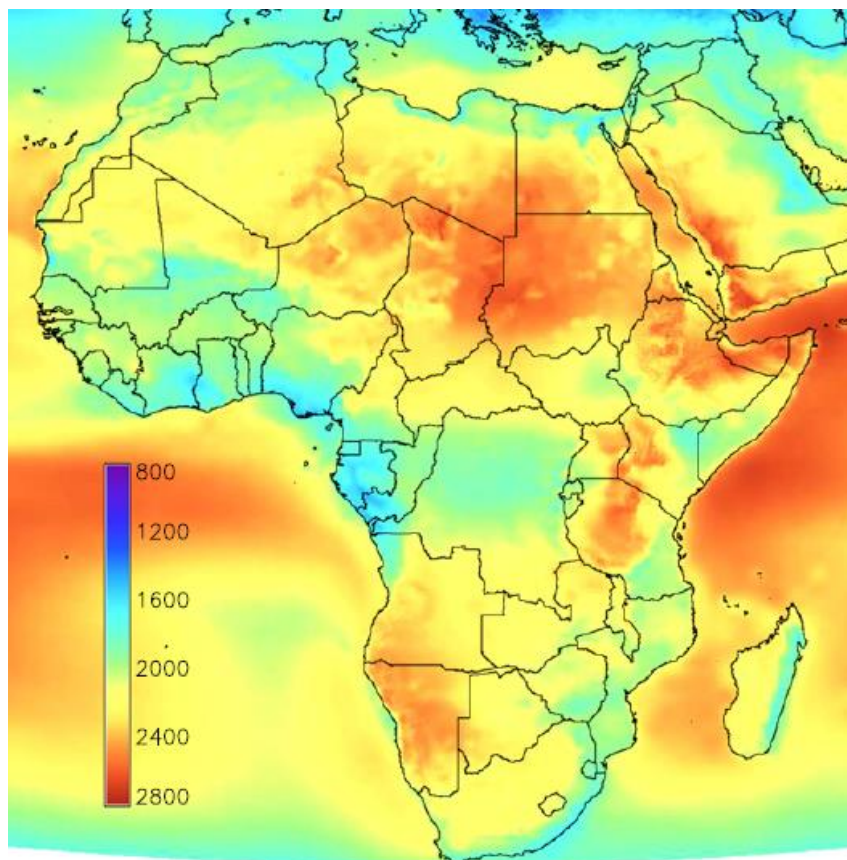

Figure 24: Map of average annual global horizontal irradiation of Africa using PVGIS-3 in kWh/m2 (Huld, 2012:1811)

An interesting occurrence is seen in Figure 25 and Figure 26. The ratio between the global irradiance and diffuse irradiance is higher for July than for January, essentially allowing for a higher global irradiance in winter in the winter than in the summer.

While one would expect the opposite to be true, this phenomenon can be explained by considering that the cloud cover in the summer in Potchefstroom is much higher and more frequent than in the winter, as summer is the rainfall season for this region. A higher cloud cover leads to more diffusion of light rays in the cloud cover and less light reaching the ground, leaving less radiation to be absorbed at the receiver.

As would be expected, the global clear-sky irradiance for January is higher than for July, as no cloud cover or diffuse irradiance is taken into account.
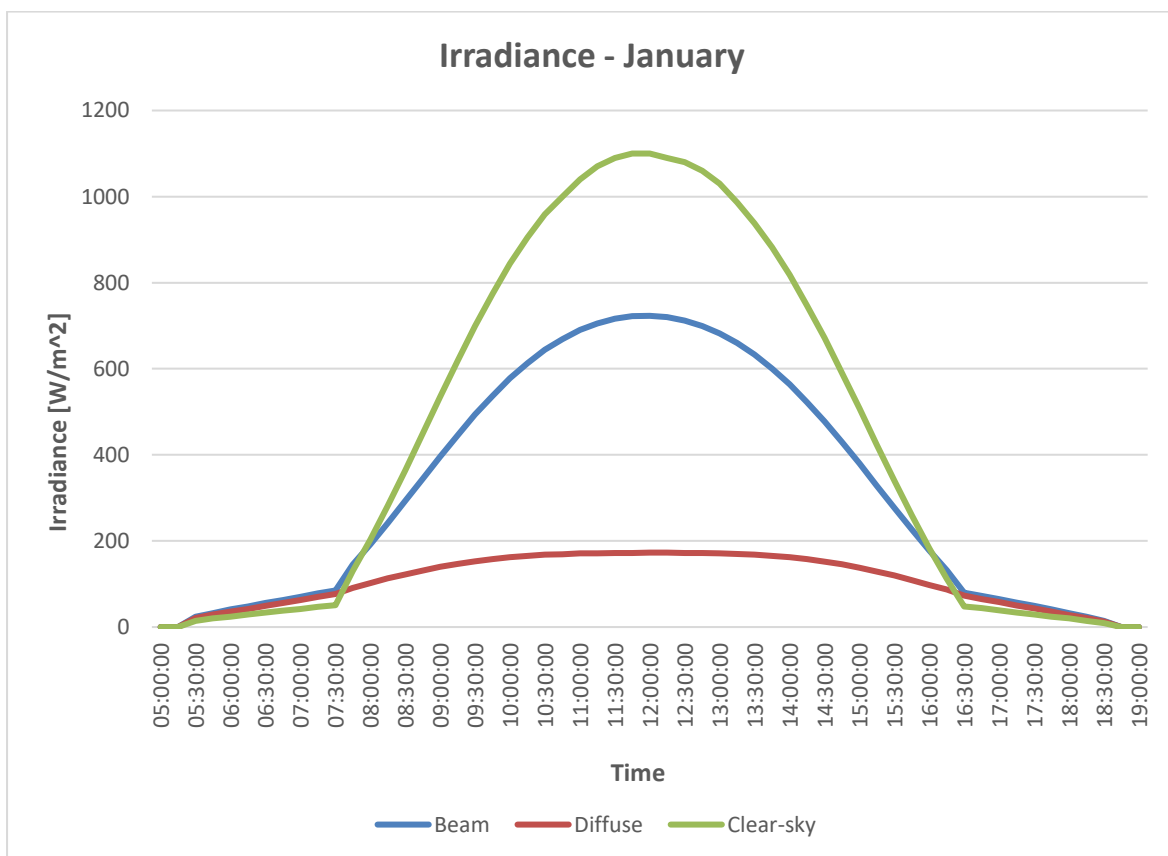

Figure 25: Graph showing the solar irradiance during the day for January
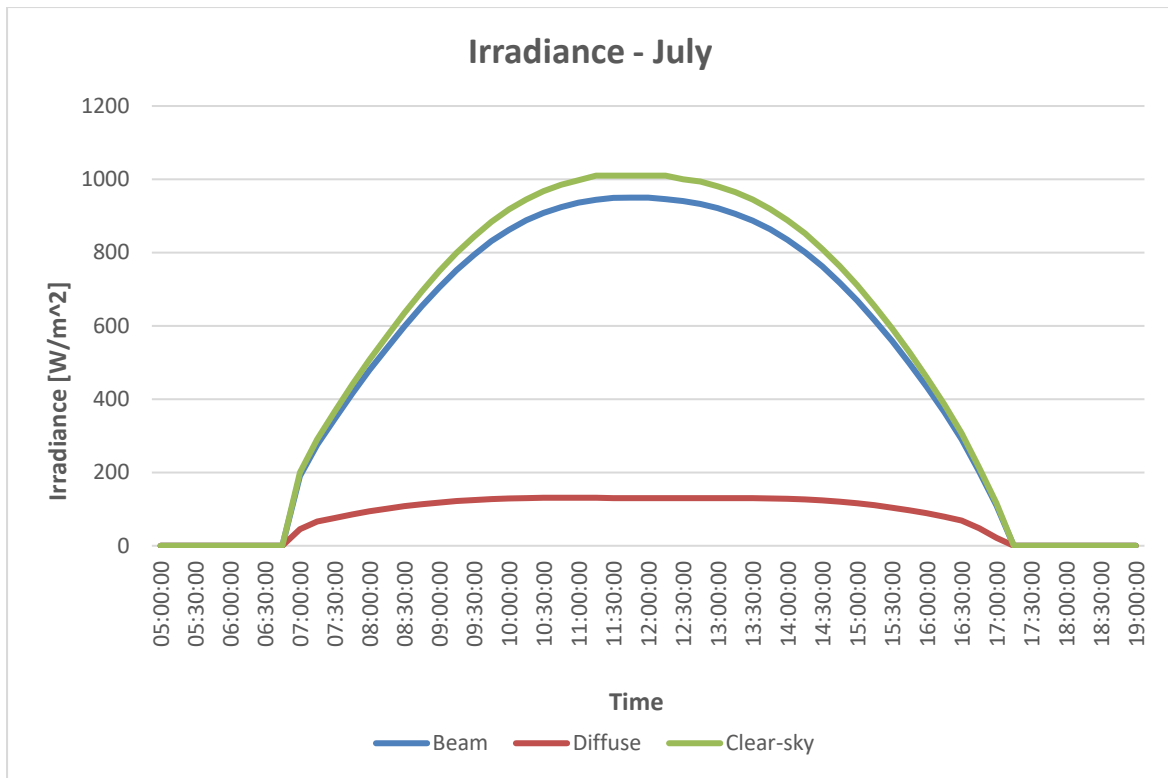
Figure 26: Graph showing the solar irradiance during the day for July

4.5 CPC thermal performance

Using equation (3.3.1) to equation (3.3.10) the useful energy gain, Q_u, and instantaneous efficiency, η, can be calculated. Table 2 contains the property values present in these equations that are needed in order to solve them.

Figure 27 shows the maximum useful energy gain for every month and is determined by the maximum midday irradiance for each month. When observing the data for cloudy days, the same phenomenon as in chapter 4.4 can be seen, with the trend following an opposite path than one would expect. Again, this is due to cloud coverage, and from this data it is clear that September is the month with the least cloud coverage in Potchefstroom.

Figure 28 shows the total useful energy gained in a day throughout the year. For both cloudy days and clear-sky days, the energy gained in the summer is significantly less than in the winter. While the total energy gained also suffers in the summer due to cloud coverage, the total exposure time to the sun also has a significant effect here. While there are more hours of daylight in the summer, the sun spends much of that time behind the East-West plane, from where the light cannot be absorbed by the North-facing receivers, leading to less total energy being absorbed throughout the day.

Table 2: CPC properties useful to the evaluation of thermal performance

| Properties	Symbol	Value	Unit
Receiver outer diameter	Do	0.0318	m
Receiver outer diameter	Di	0.0258	m
Thermal conductivity of pipe	k	53.661	W/mK
Thermal conductivity of fluid	kf	0.1362	W/mK
Nusselt number	Nu	4.364	-
Emissivity of receiver	εr	0.65	-
Average number of reflections	n	0.6	-
Mirror reflectivity	ρ	0.9	-
Cover transmissivity	Tcover	0.85	-
Receiver absorptivity	αr	0.96	-
Mass flow	m	0.03	kg/s
Specific heat	cp	2188	J/kgK
Output temperature (estimate)	To	105	°C
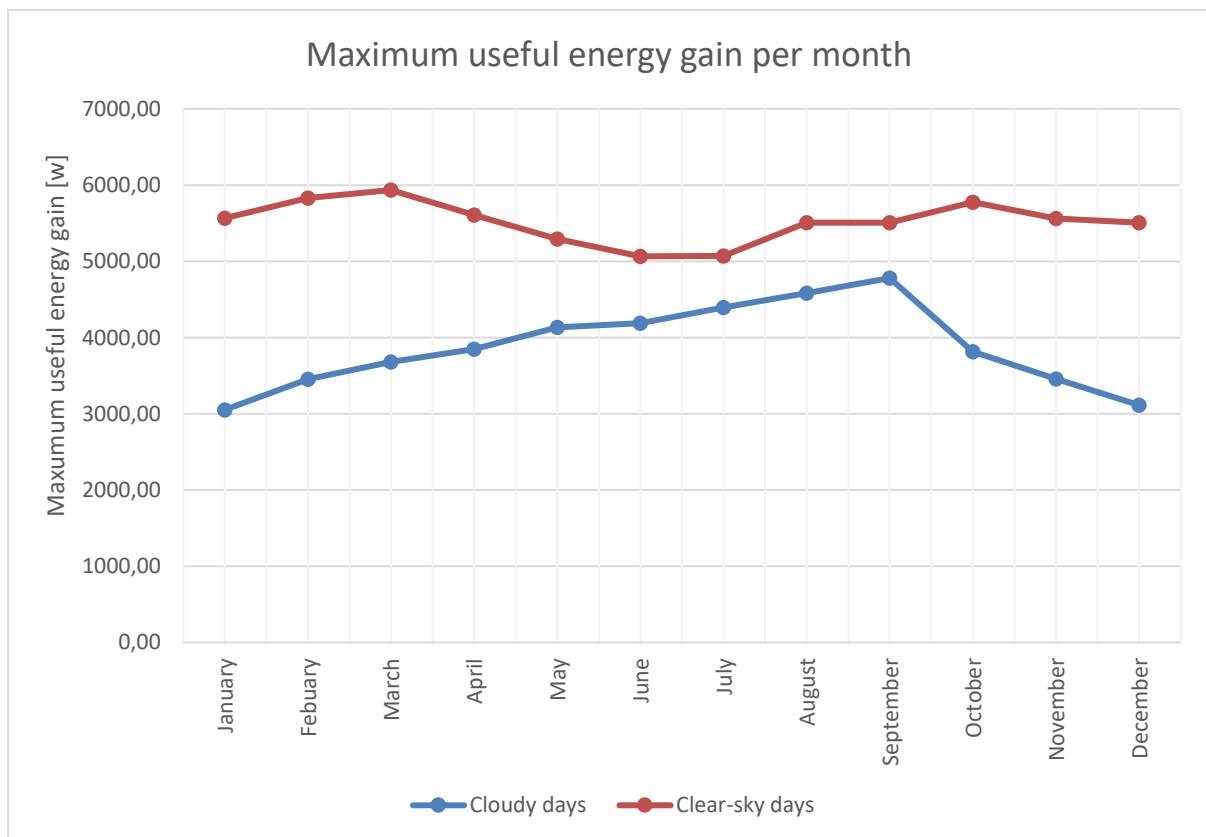
Figure 27: Graph showing the maximum useful energy gain throughout the year
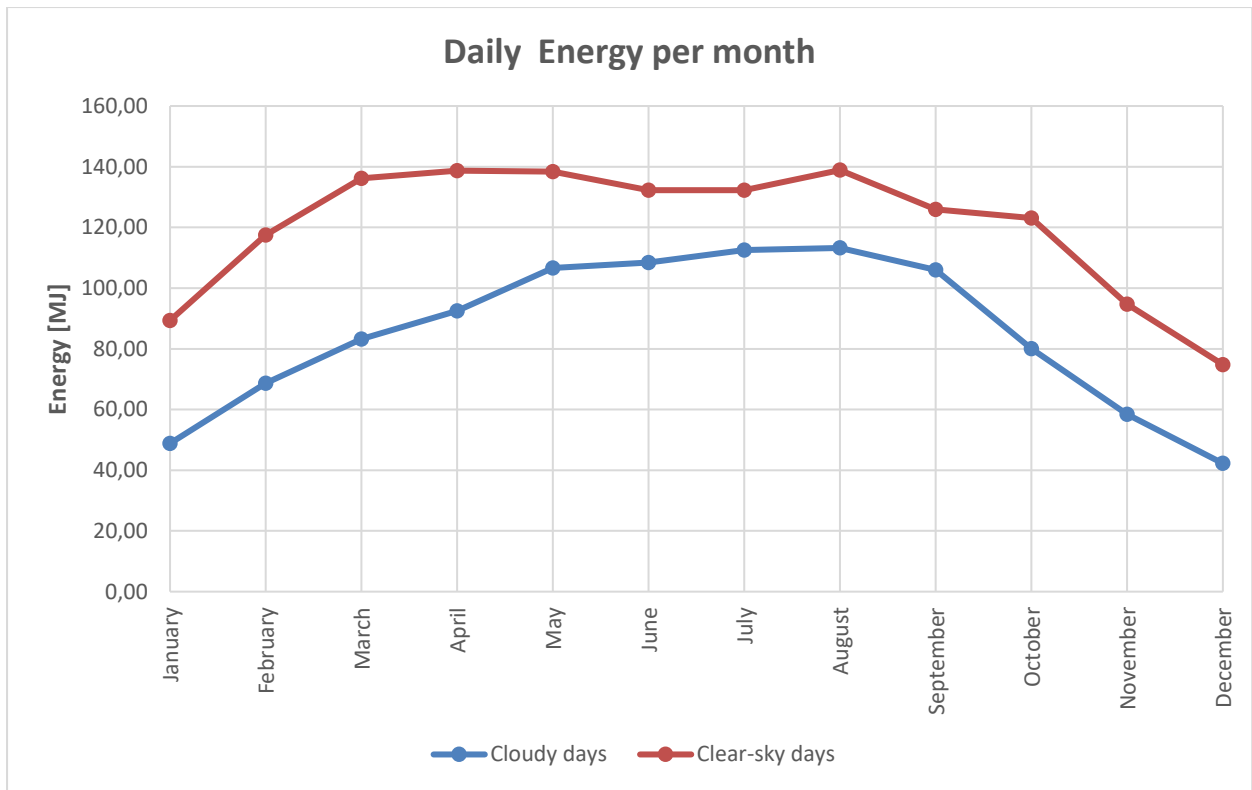
Figure 28: Graph showing the total useful energy in a day throughout the year

In order to verify these theoretical results, the values from Figure 27, which was calculated with *Microsoft Excel*, are compared with values calculated with the *Engineering Equation Solver (EES)*, as shown in Table 3. As can be seen from the table, the maximum useful energy gain values for cloudy days are practically identical, further confirmed by Figure 29 and Figure 30.

Table 3: CPC properties useful to the evaluation of thermal performance

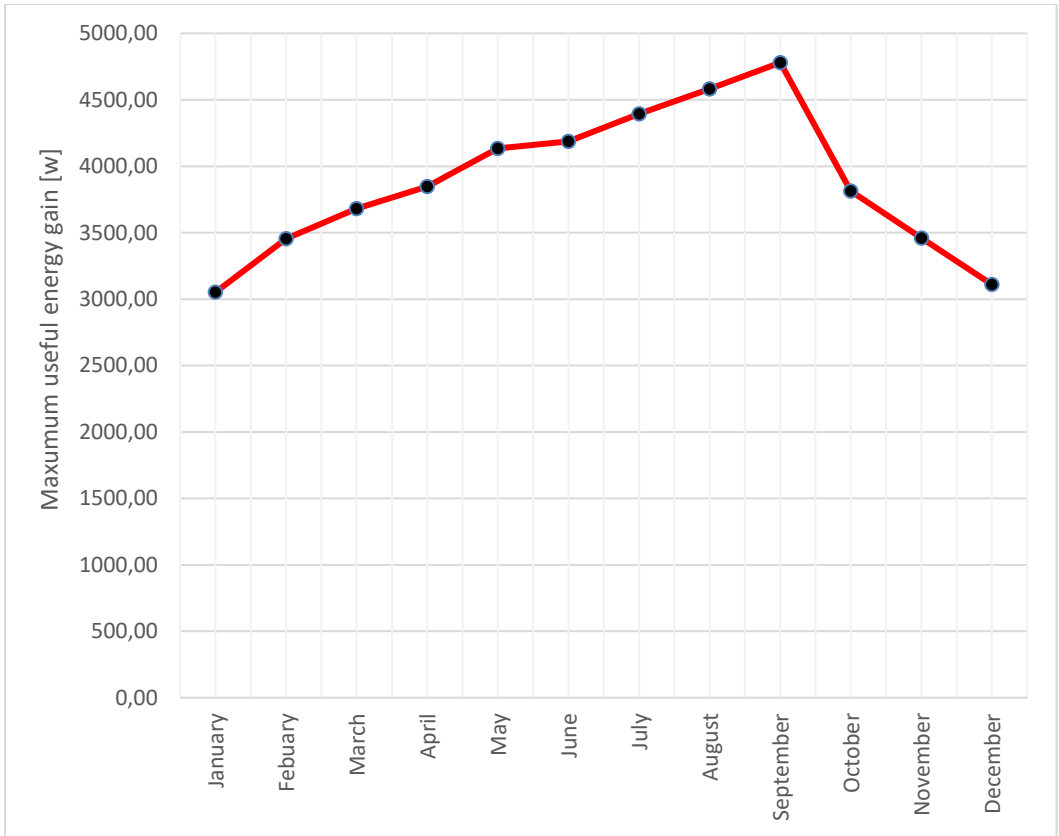| Month	G_t [W/m^2]	G_d [W/m^2]	Qu [W] (Excel)	Qu [W] (EES)
January	723	173	3051,87	3052
February	794	164	3455,08	3455
March	853	198	3681,45	3681
April	860	154	3847,85	3848
May	901	132	4134,20	4134
June	912	130	4187,18	4187
July	950	130	4395,38	4395
August	983	129	4581,72	4582
September	1030	146	4780,08	4780
October	866	177	3814,22	3814
November	794	164	3459,63	3460
December	729	162	3111,23	3111

Figure 29: Graph showing the total useful energy in a day throughout the year for cloudy days from Excel
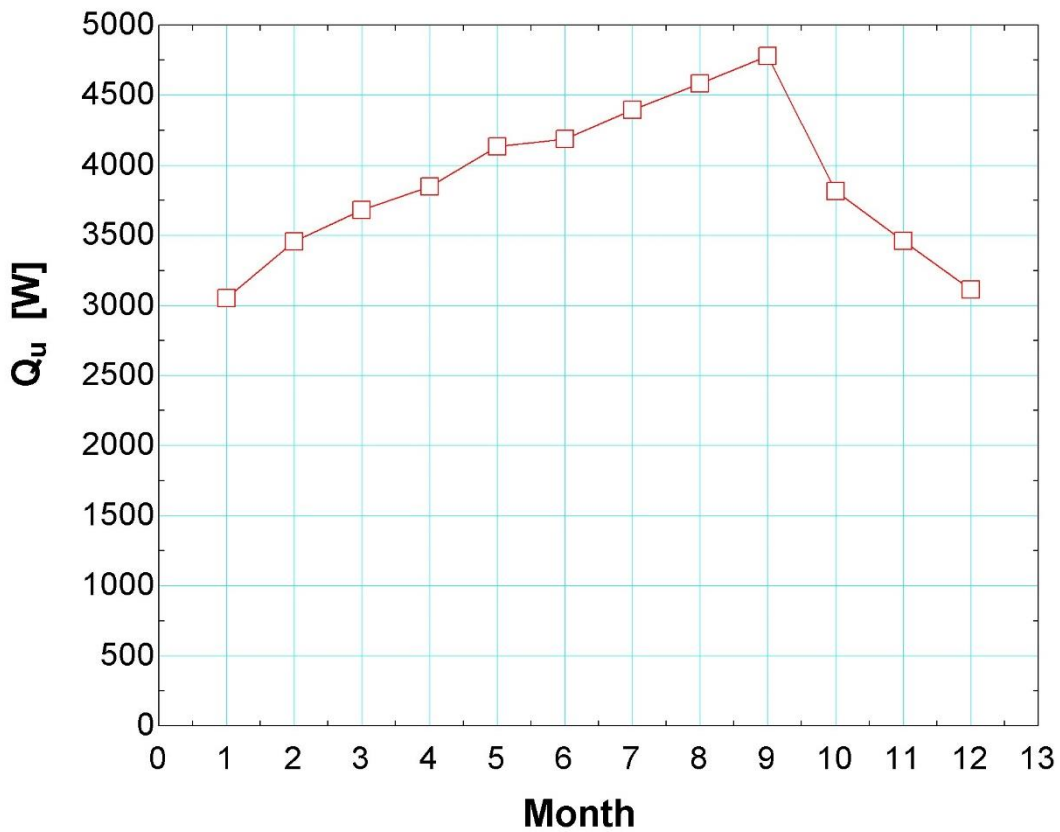

Figure 30: Graph showing the total useful energy in a day throughout the year for cloudy days from EES

4-40

4.6 Geographic applicability

At midday, the collector, with a half-acceptance angle of 28°, will be able to concentrate solar rays at an incidence angle of between 88° and 32°. Use of this collector design would not be recommended at latitudes where the solar altitude angle is higher than 88° in the summer midday or lower than 32° during the winter midday. Using the model from Chapter 4.1, the maximum and minimum solar altitude angles for different latitudes were calculated, as shown in Figure 31, which shows that this collector would be unsuitable for latitudes above 25.5° South and below 36° South.

From the solar map shown in Figure 24 it can also be concluded that the collector would be unsuitable for placement in the coastal areas of South Africa, as the irradiation input would be up to 33% less than it was designed for. Thus, Figure 32 shows a map of the suitable region for this collector design, as recommended by this study.
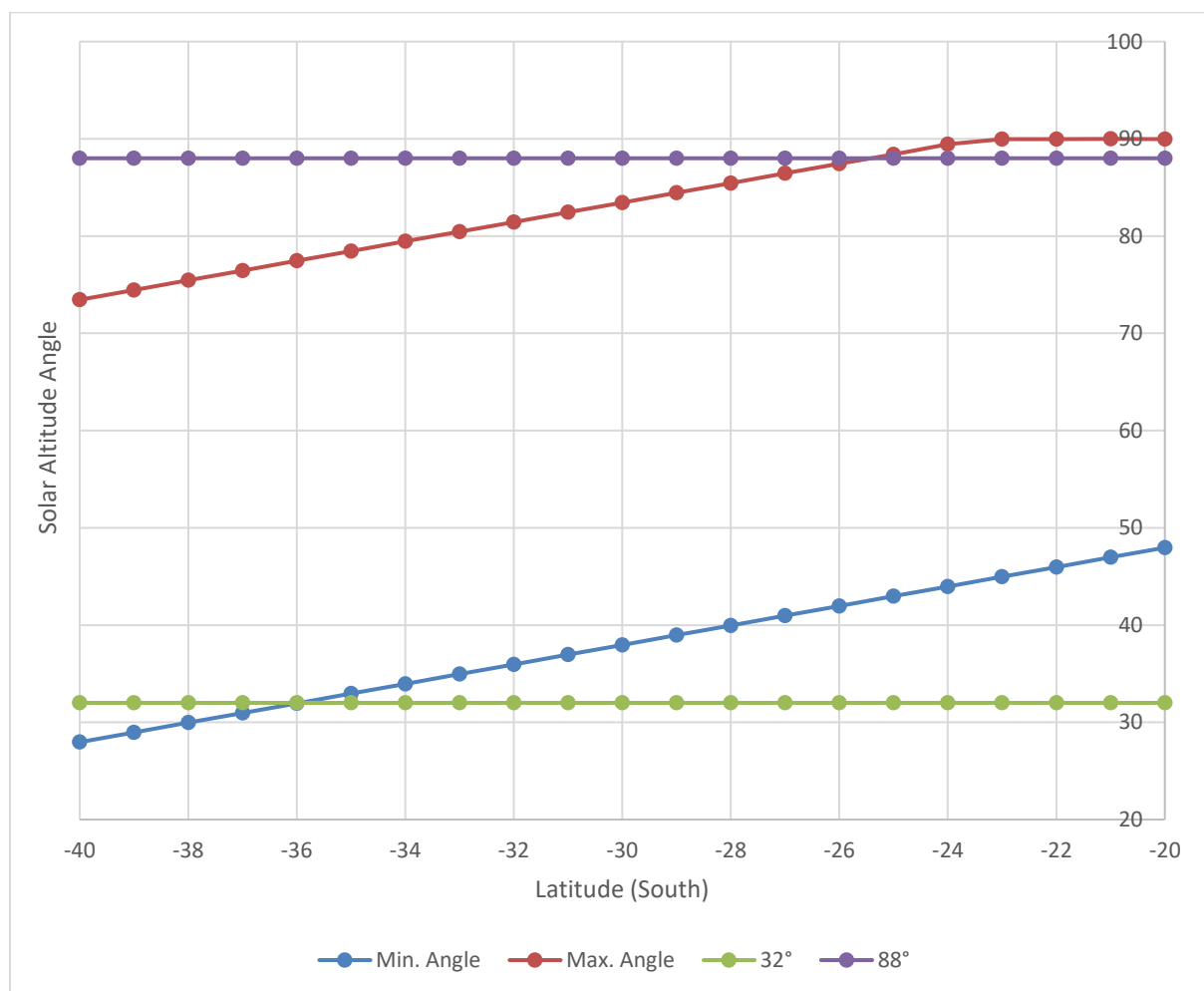

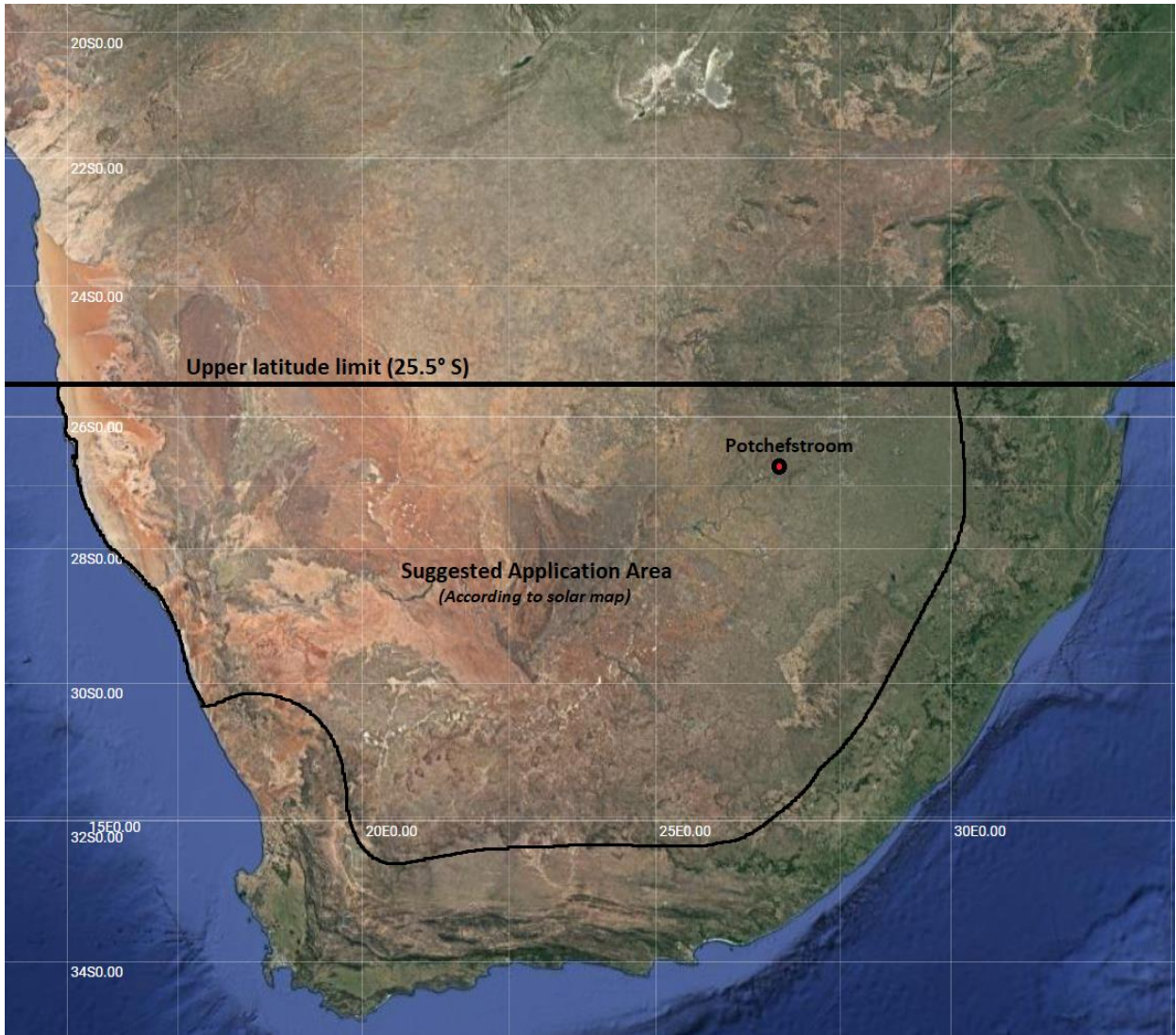**Figure 31: Graph showing the solar altitude angles for different latitudes**

Figure 32: Map showing the suggested application area of the collector designed in this study

5 Collector design and fabrication

This chapter discusses and describes the CPC collector design choices and fabrication methods.

5.1 Concentrator design

The reflector profile calculated in chapter 4.2 was used to design the compound parabolic concentrator shown in Figure 33. The reflector is made from a 0.5 mm thick polished aluminium sheet, bent into the CPC profile with a small radius added in the middle to simplify construction.

The reflector is held at both ends by end caps, with a few support ribs and inner supports to stabilize the concentrator. These components are laser cut from Superwood to decrease the weight of the unit.

A Perspex cover is added to the top to minimize convection heat losses and prevent dirt from settling on the reflector. A mild steel stabilizing plate is fixed to the bottom of the unit to stabilize and balance it.

Finally, a mild steel connecting arm is fixed to the unit, where a crank mechanism will connect to it, allowing the CPC unit to rotate.
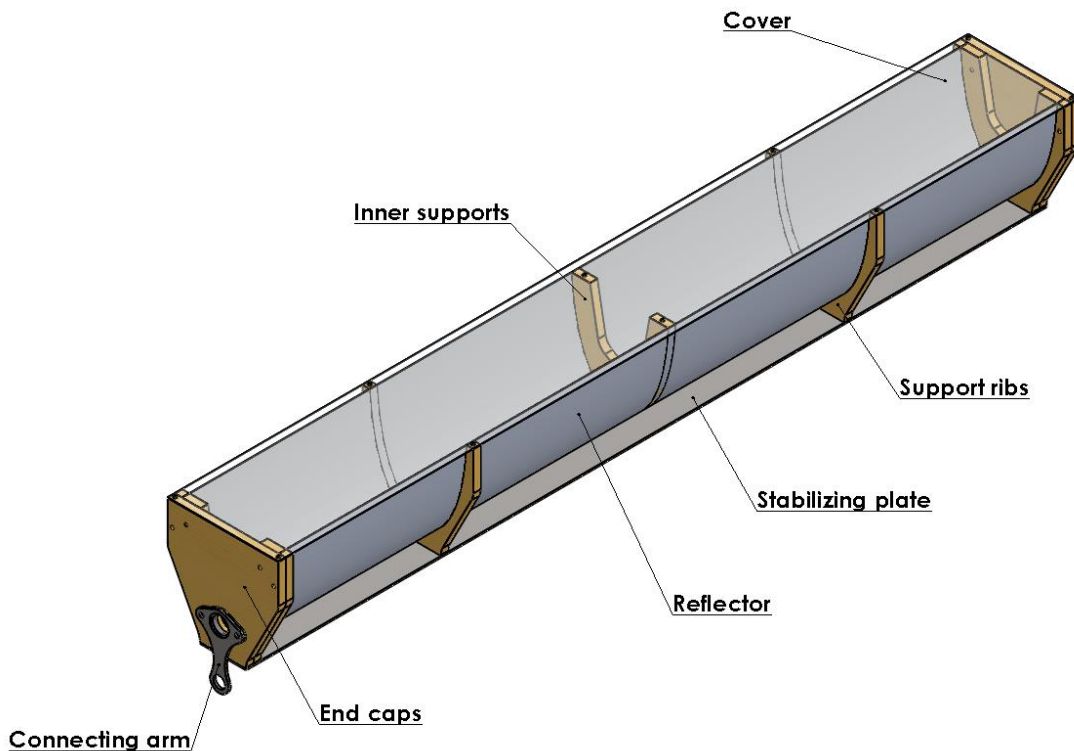

Figure 33: Drawing of the compound parabolic concentrator assembly

5.2 Tracking mechanism design

The sun-tracking employed in this this design involves using a pendulum to time the rotation of an escapement wheel. The escapement wheel is connected to a train of gears with a gear ratio of 720:1, slowing the speed of rotation down 720 times, to the speed that the collectors will be rotating at. The gear train is connected to a weight wheel, from which the weights that drive the gears hang by cables.

In turn, a tracking shaft is rotated and turns a wheel that drives a crank rod. The rod is connected by plates to every connecting arm on every one of the 28 CPC units, allowing them to be rotated upwards from 10° with the horizon to 60°.

The pendulum assembly shown in Figure 34 consists of a clamp, a pendulum rod and a bob. The bob is supported from the bottom and constructed from several layers of 6 mm thick bronze, layered into an aerodynamic semi-cone shape. The pendulum rod is made of mild steel with a length of approximately 1m, which translates to a pendulum period of 2 seconds.
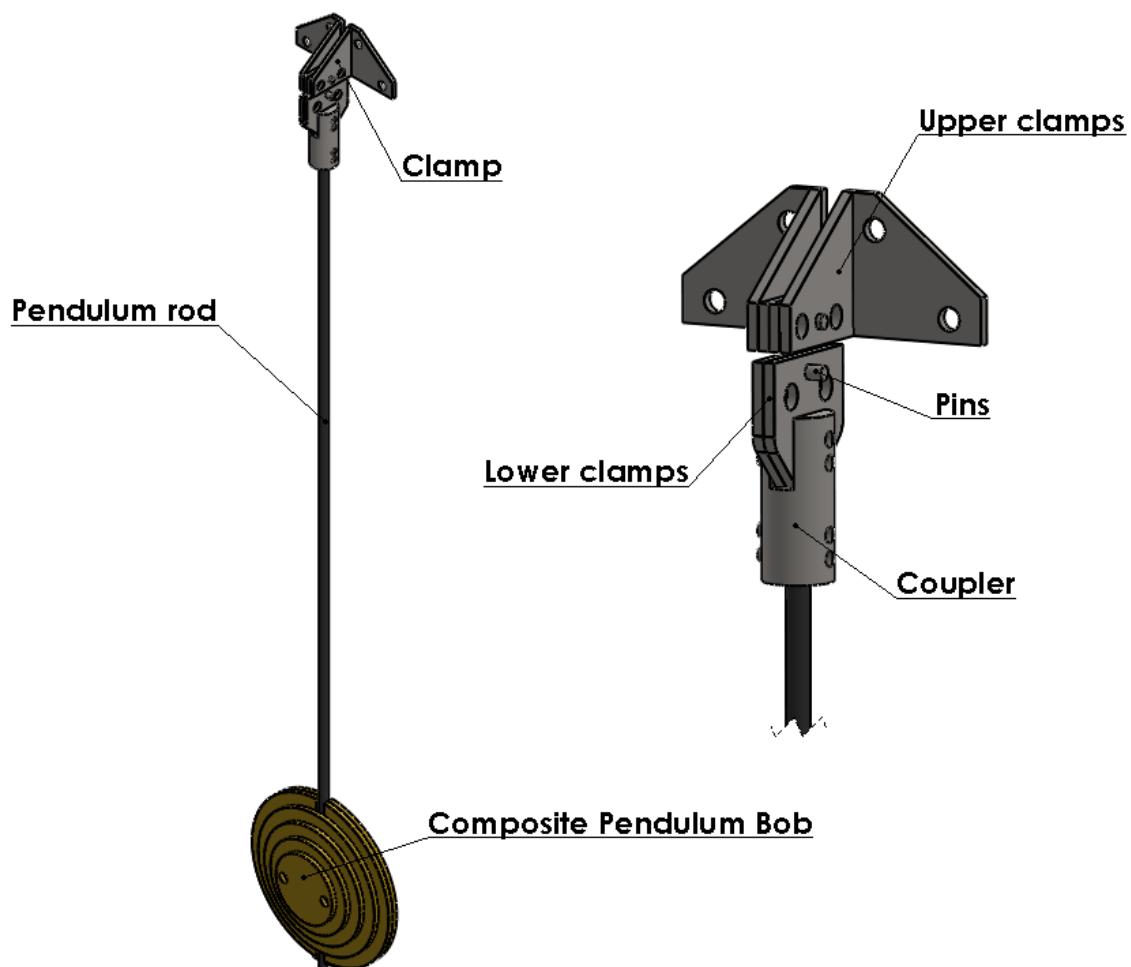
Figure 34: Drawing of the pendulum assembly

The bronze is chosen for its high thermal expansion coefficient to compensate for the expansion of the long mild steel rod, which has a lower thermal expansion coefficient, allowing the two thermal expansions to nearly cancel each other out. This keeps the bob's centre of mass at the same length from the rotation point, preventing the pendulum period from changing.

The clamps holding the pendulum to the gear box are made from mild steel and are held together by bolts and mild steel pins. Between the upper and lower clamps, a 0.1 mm thin suspension spring is clamped, allowing for the movement of the pendulum.

Figure 35 shows the gearbox to which the pendulum assembly is bolted, and which drives the rotation of the CPC units. The graham pallet translates the pendulum movement to the escapement wheel, which is specifically designed to keep the gear train in time and add extra energy to the pendulum, preventing it from losing its momentum.
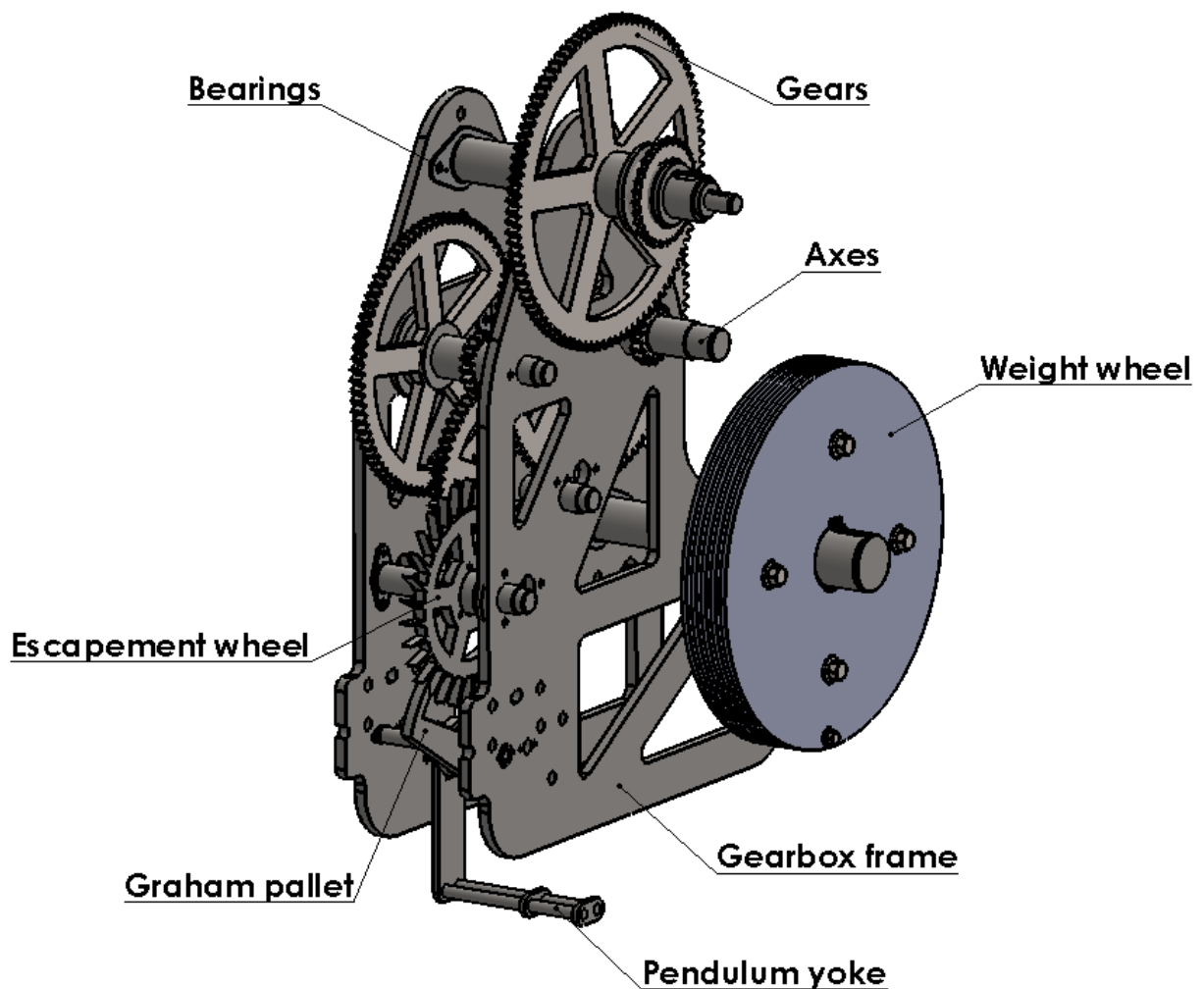

Figure 35: Drawing of the gearbox assembly

The rotational speed of 1 rpm at the escapement wheel is reduced to an eventual 1/720 rpm at the tracking shaft, which drives the rotation of the collector. *Igus* iglidur G flange bearings are used to allow the gear axes to rotate. These bushing-like bearings have a low coefficient of friction and can withstand medium temperatures, which is why they are also used in the CPC units to allow for rotation around the receiver tubes.

Cables are suspended from the weight wheel, from which the weights that drive the tracking mechanism hang. This weight wheel is constructed from layers of mild steel plate bolted together.

The crank rod mechanism that translated the rotational movement of the tracking shaft into lateral movement that rotates the concentrators, is shown in Figure 36. The crank arm and crank pin is fixed to the crank rods at this position, while the crank rods are jointed to the connecting arm of every CPC unit. As the tracking shaft and crank wheel rotates, the crank rods move laterally, pushing on the connecting arms of the CPCs, forcing them to rotate around the receiver tubes.
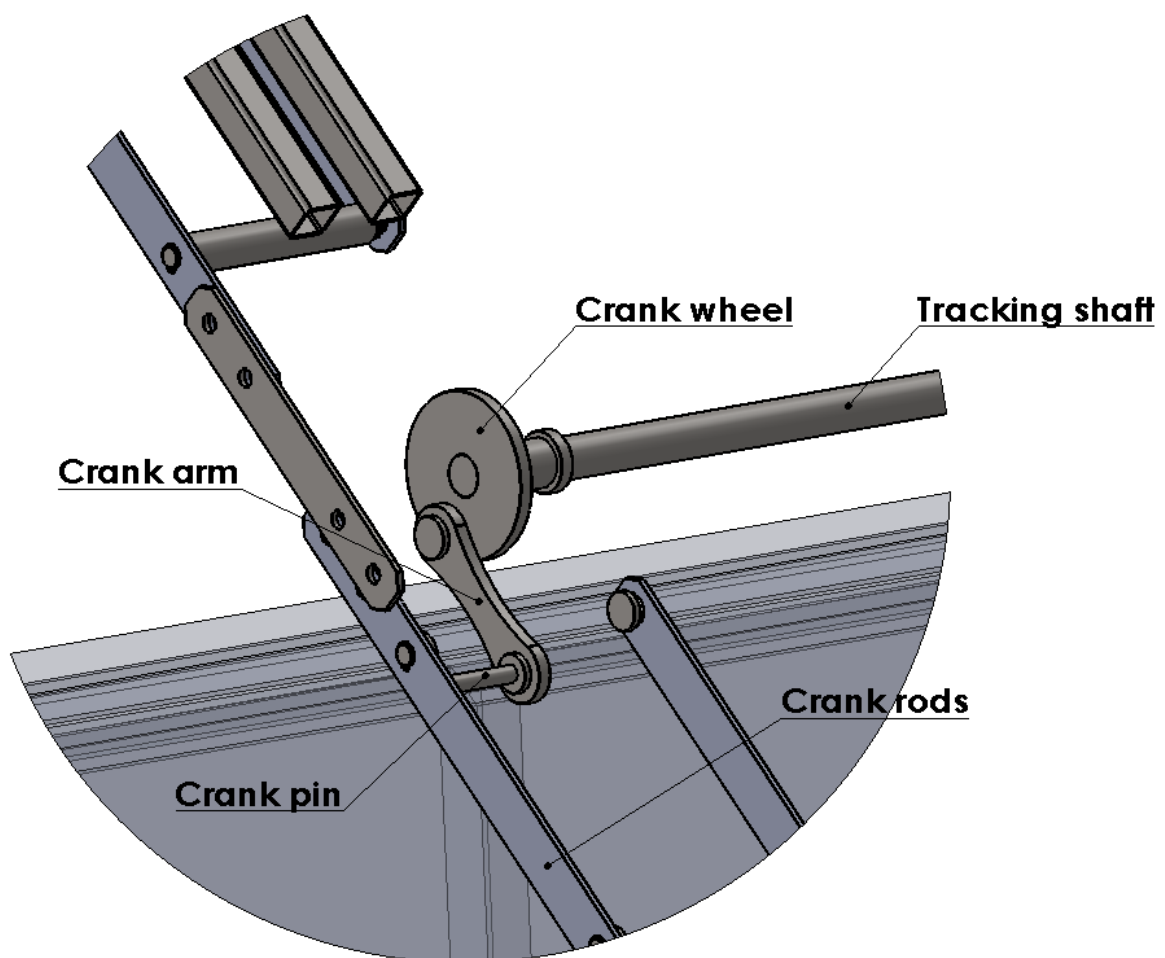

Figure 36: Drawing of the crank rod assembly

5.3 Complete collector design
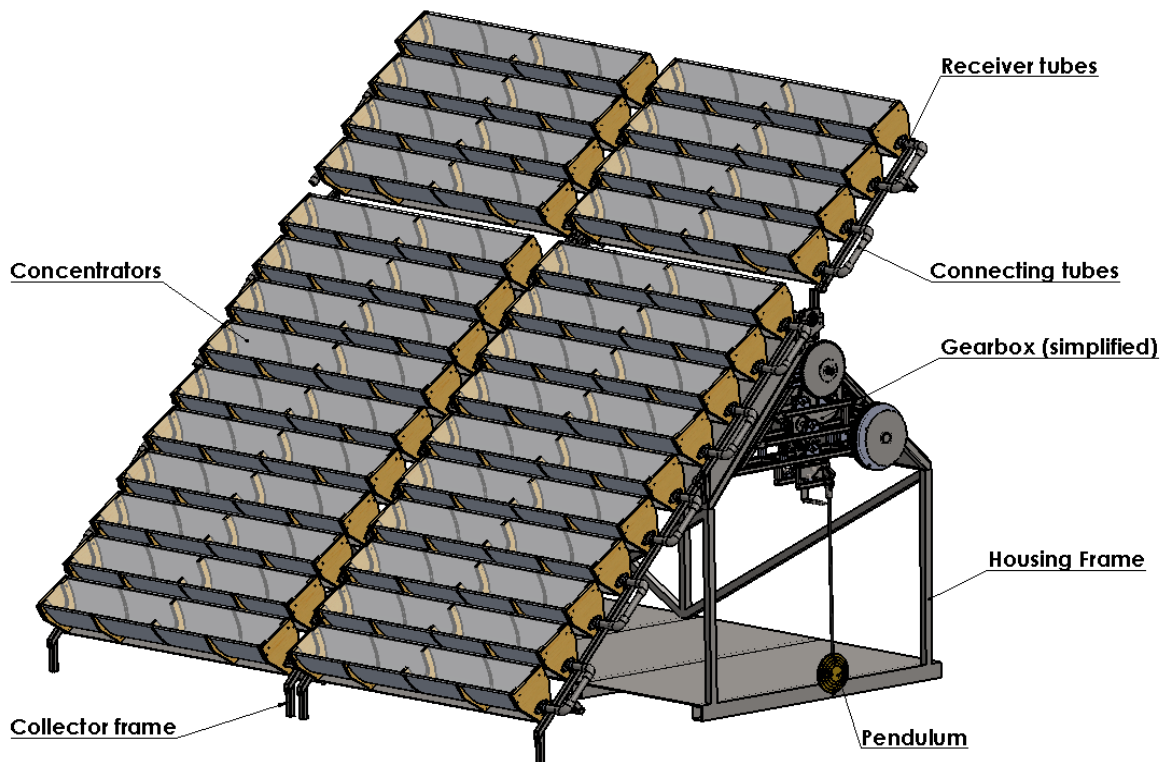
Figure 37: Drawing of the collector assembly

Figure 37 shows the complete collector and tracking design (the gearbox was simplified in the model due software limitations). The housing frame is the pre-built structure on top of which the collectors are built and which will house the aqua-ammonia absorption refrigerator components. For perspective, the height of the housing frame is 1.75 m.

The receiver tubes are connected in a serpentine fashion, allowing the fluid to move through all the concentrators before reaching the top. The top set of collectors are hinged and can be folded down to the other side of the roof, while the bottom set of collectors are also hinged and can be folded up against the side of the housing frame when it is on ground supports.

5.4 Fabrication details

The receiver tubes were painted with AeroSpec 250 Solar Collector Coating, which increases the absorptivity of the tubes, while decreasing the emissivity. This leads to more heat absorption and less heat loss.

All wood components were given two coats of a waterproof wood treatment, as shown in Figure 38, to prevent the wood from absorbing too much water, and expanding or rotting.

Any mild steel components, including frames, gears, shafts and plates were painted with Polycell EndRust, a rust converter and anti-rust coating, to prevent the components from rusting, and to remove rust from the housing frame, as shown in Figure 39.

Lastly, all moving part were lubricated with Q20.

Figure 38: Wood components after being coated with waterproof wood treatment
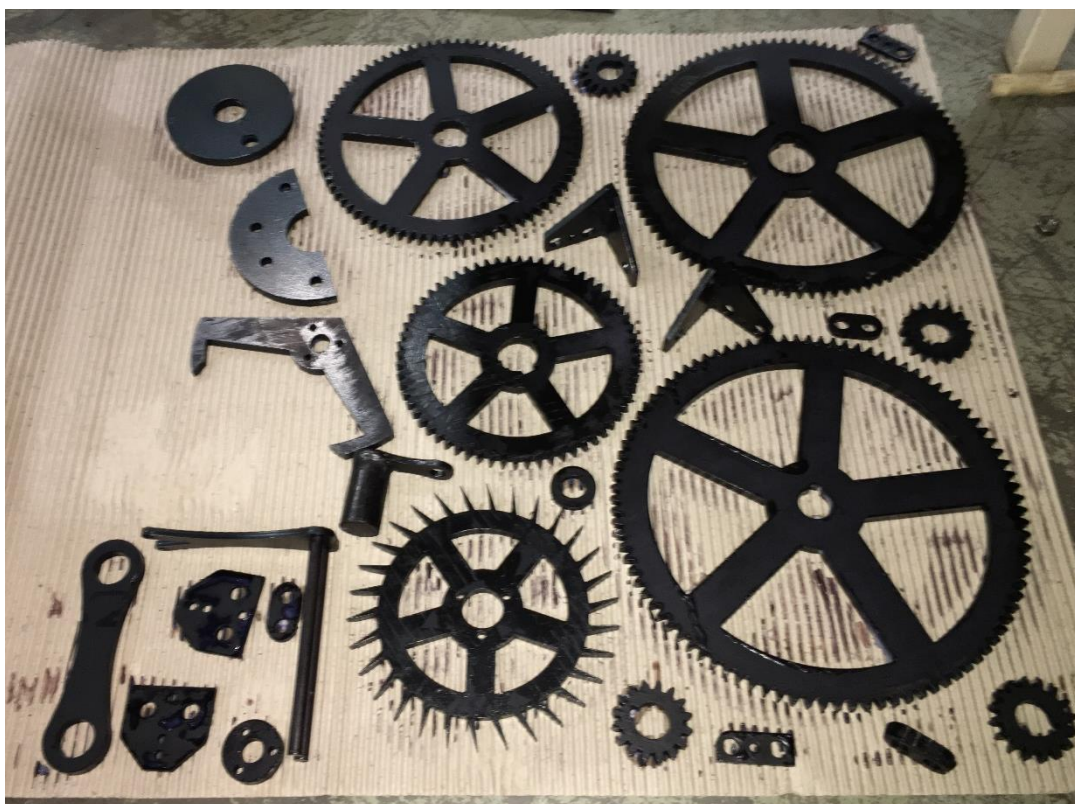
Figure 39: Mild steel components after being coated with anti-rust coating

5.5 Cost of construction

The total cost of the materials and labour for the construction of the tracking concentrating parabolic collector amounts to R 26 985.95. This cost includes the cost of the materials, coatings, laser cutting, water-jet cutting, sprockets, chains and bushing bearings. The total cost of the materials for a stationary CPC without the tracking mechanism would amount to R 18 361.28.

As shown in Figure 27 in Chapter 4.5, the designed CPC would theoretically be able to deliver almost 6000 [W] on a clear sky day. The average cost of a 300 [W] photo-voltaic solar panel in South Africa is about R 2 100.00. The total cost of the equivalent number of PV panels would be approximately R 42 000. This would exclude the cost of installation and the electronics necessary to heat the bubble pump. Thus, there is clearly a cost benefit to constructing a CPC collector instead of using PV panels.

6   Experimental Setup

In this chapter, the experimental setup is discussed.

6.1   Measurement equipment

The Endress+Hauser Memograph M RSG40 graphic data manager is used to log the necessary data. All thermocouples and flow meters can be calibrated with this piece of equipment.

Type-T thermocouples are used to measure the inlet, outlet and ambient temperatures. These thermocouples have a range of between -50°C and 200°C and the wires and made from copper and constantan. The thermocouples were calibrated by submerging them in an ice bath, slowly increasing the temperature of the water, and making adjustments on the logger if the thermocouple shows a different temperature than the actual temperature, as shown in Figure 40 and Figure 41.

To measure the mass flow in the system, a Gems Sensors Nylon 12 Liquid Sensor 173936-C flow meter is used. This flow meter has a range of 0.5 – 5 L/min and runs at 24V.
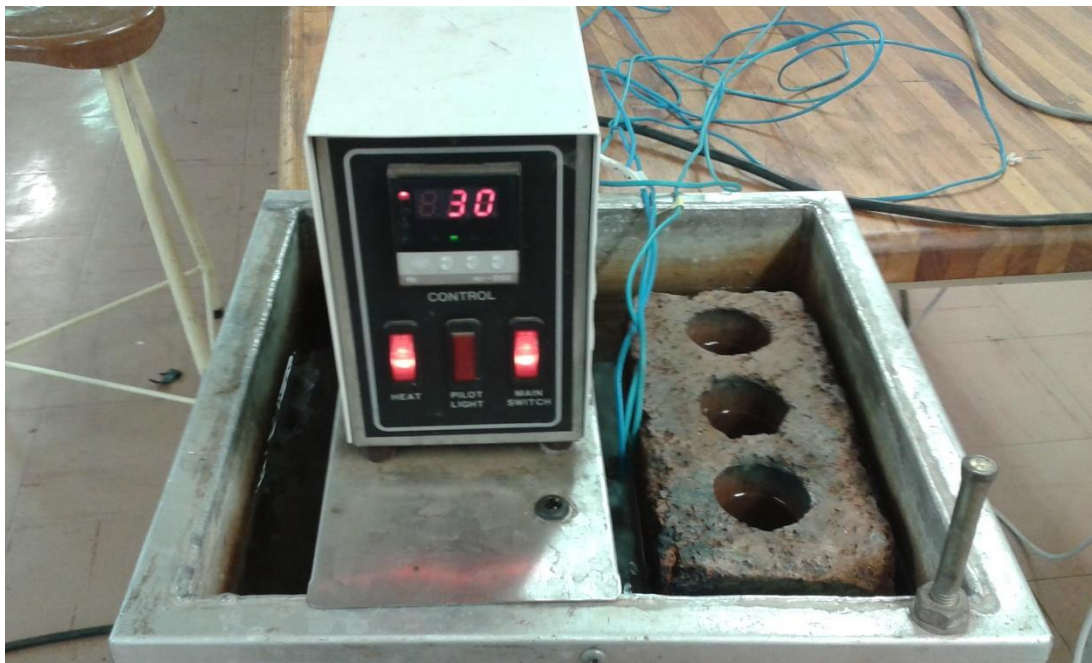

Figure 40: Thermocouples submerged in ice bath during calibration
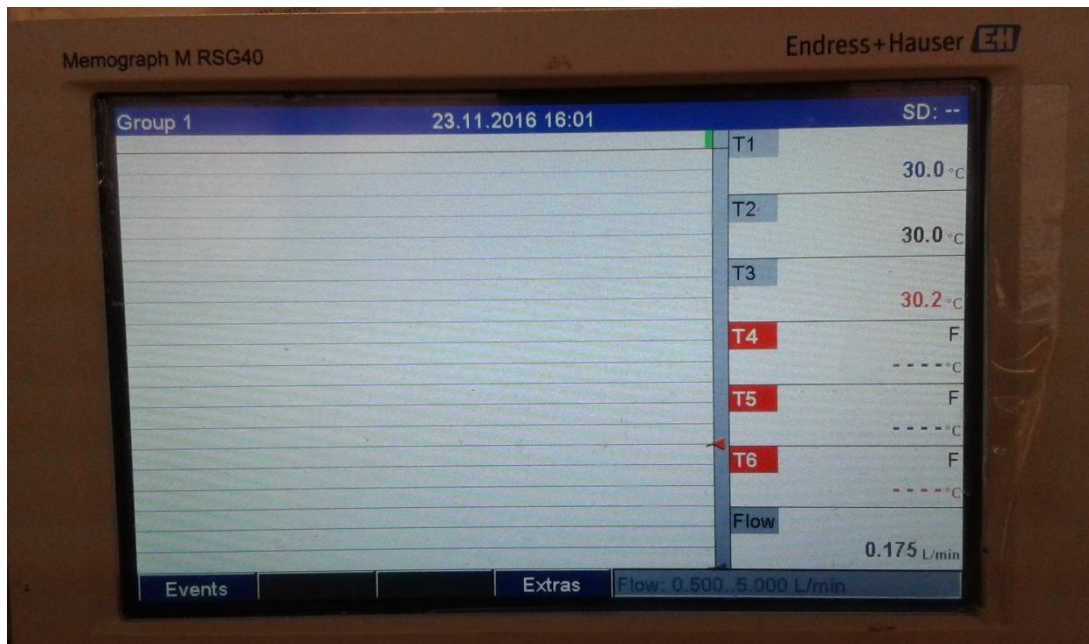
Figure 41: Example of calibration needed for T₃

6.2 Test setup

Measurements on the system were taken from 29 March 2017 to 30 March 2017.

As the rest of the aqua-ammonia absorption refrigeration system had not yet been constructed at that time, a closed loop of piping was created for the purposes of this experiment, in order to validate the theoretical results, as shown in Figure 42 and Figure 43. The piping leaving the collector outlet was submerged in an ice bath in order to lower the inlet temperature. An expansion pipe was also affixed to the collector outlet, to compensate for liquid expansion, and prevent the internal pressure of the piping to increase.

An ITS TS510PV 12V circulation pump was connected to the piping to induce flow in the system, connected to a valve to control the flow through the system, as shown in Figure 44. An SDDirectPro Enersol 15W solar panel was connected to the circulation pump to allow it to run.

Engen Multipurpose Antifreeze was used as the fluid in the system due to having a boiling point of 150°C and being widely available.

The fully set up system can also be seen in Figure 45.

Figure 42: Diagram indicating the test setup

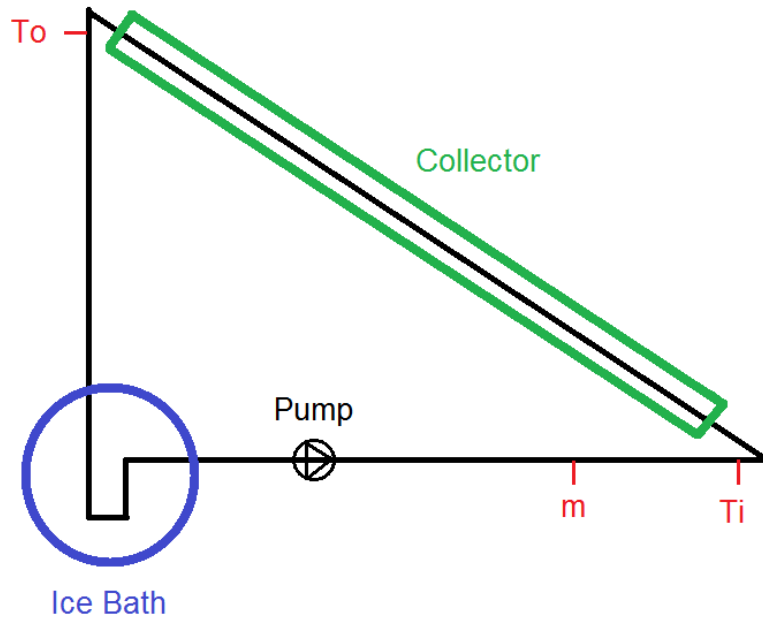**Figure 43: Photo indicating the test setup**

Figure 44: Photo indicating the ice bath and circulation pump

Figure 45: Photo indicating the overall view of the experimental setup

7 Results

A full day of measurements was captured for 29 March 2017. The measured data is represented in Figure 46. Cloud cover was present on this day and the flow through the system was kept at approximately 0.3kg/s. Ice was continually added to the ice bath in order to keep the inlet temperature low and simulate the lower inlet temperature that would enter the collector if connected to a full aqua ammonia absorption refrigeration system.

Anomalies are clearly present in the data. The first anomaly occurs from approximately 08:00 to 09:00, where the outlet temperature should be rising, but does not. This was due to a blockage in the piping, which caused the outlet temperature to rise quickly as no flow was taking place. The blockage cleared up at around 09:00. The second and largest anomaly starts at approximately 13:00 and lasts until 14:00, when a leak originated in the piping, causing hot fluid to be lost leaving the top thermocouple open to the air. The leak was repaired and flow resumed when the lost fluid was replaced. The final anomaly at approximately 16:00 was also due to a small leak, which was quickly repaired in about 15 minutes.
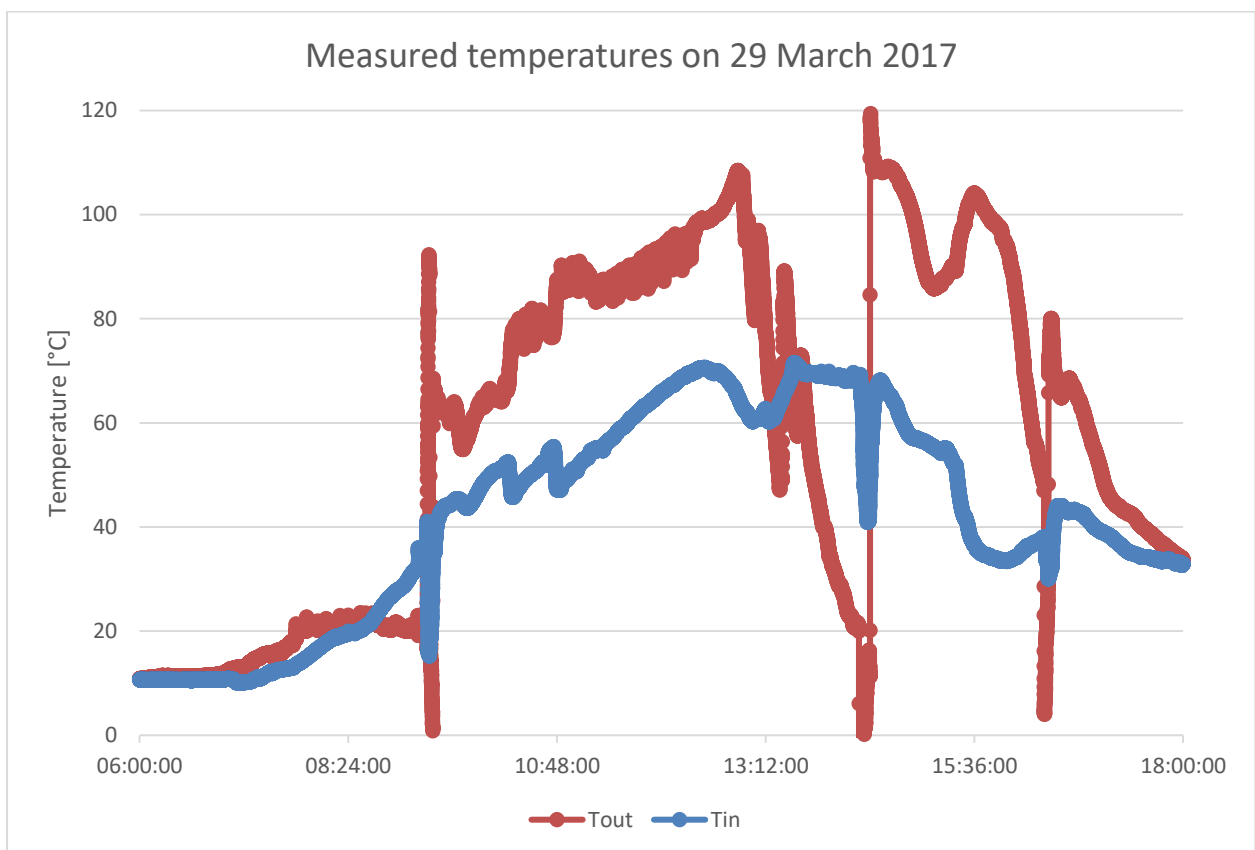

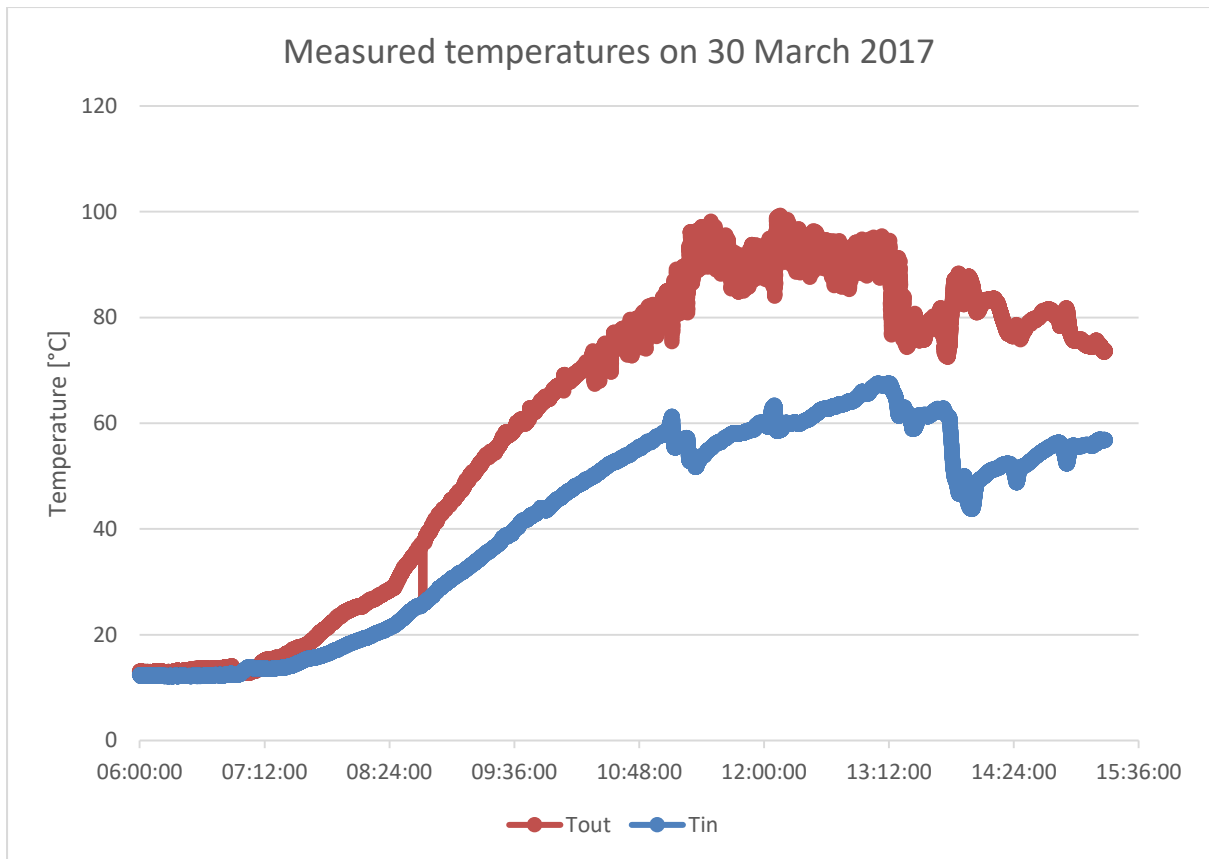**Figure 46: Graph indicating the temperatures measured on 29 March 2017**

Figure 47: Graph indicating the temperatures measured on 30 March 2017

Another day of measurements was captured on 30 March 2017; however, the data was only captured until 15:30. The measured data is represented in Figure 47. Cloud cover as well as rain was present on this day and the flow through the system was kept at approximately 0.3kg/s. On this day, the ice bath was only filled with ice once at 06:00, with no further ice added during the day.

Rain started to fall at 12:20, which greatly increased the cloud cover and reduced the available solar rays. The rain stopped at 14:05. Another leak occurred on this day at approximately 14:00, but was quickly repaired, allowing the flow to continue.

Throughout the two days of measurement small, sudden jumps can be seen in the temperatures. This can be explained by the circulation pump turning off from time to time. It is unclear why this occurred, however the effect of this can be seen as the flow stops and the fluid stagnates, allowing it to quickly rise in temperature, before the pump switches on again and the temperature drops as normal flow resumes.

Over the two days of measurement, temperatures of over 90°C were achieved, with the maximum temperature at 109°C. As the required temperature was reached, it was decided that the objective for this study was reached, and that no further testing was required.

8   Discussion

Using equation (3.3.2), the actual useful energy gain can be calculated from the measured data, as shown in Figure 48 and Figure 49. The areas of the graph where the values decrease suddenly is caused by the anomalies discussed in Chapter 7.

The data from 29 March 2017 shows that the maximum actual energy gain is 4462.33 W, while the energy gain at midday is 1811.66 W. When this energy is compared to the theoretical maximum useful energy gain for a cloudy day in March of 3681.45 W, and the theoretical energy gain for a cloudy day in March in Figure 48, it can be seen that, while neglecting the anomalies, no clear correlation between the two can be seen.

The data from 30 March 2017 shows that the maximum actual energy gain is 2879.41 W, while the energy gain at midday is 1822.61 W. When this energy is compared to the theoretical maximum useful energy gain for a cloudy day in March of 3681.45 W, and the theoretical energy gain for a cloudy day in March in Figure 49, it can be seen that, while neglecting the anomalies, no clear correlation between the two can be seen.
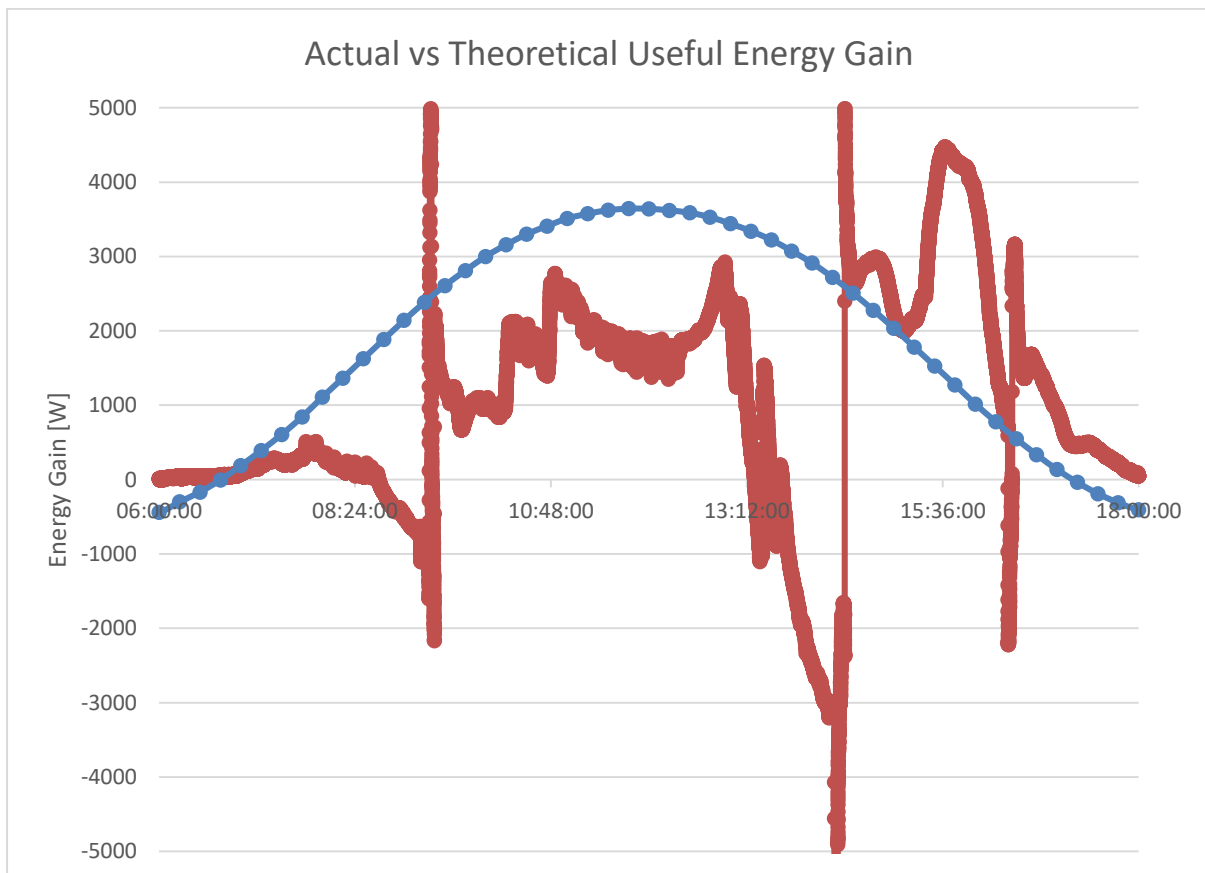

Figure 48: Graph comparing the actual and theoretical useful energy gain for a cloudy day on 29 March
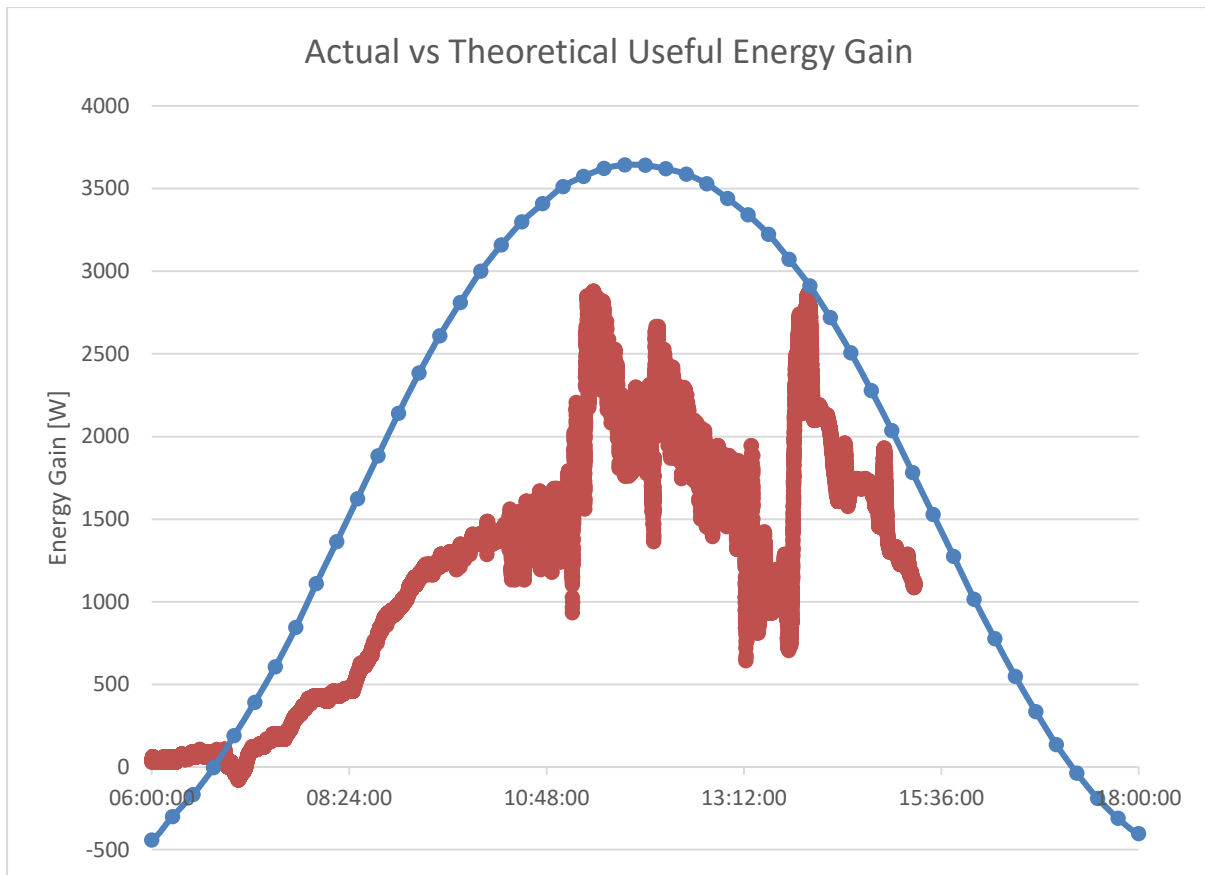
Figure 49: Graph comparing the actual and theoretical useful energy gain for a cloudy day on 30 March

To more clearly compare the theoretical and experimental values, Figure 50 and Figure 51 show the cumulative experimental heat gain versus the cumulative theoretical heat gain for 29 March 2017 and 30 March 2017, respectively. In these graphs, a correlation between the mathematical model and experimental values becomes clearer. As expected, the experimental values are lower than the theoretical values.

The difference between the values can be explained by several reasons. Primarily, the differences are caused by leakages that occurred during measurement. During the time it took for the leaks to stop and be repaired, no heat was absorbed. Some of these leaks occurred during the hottest time of day as the fluid expanded, thus losing time to absorb heat at the time of peak solar irradiance.

Alternatively, some dust may have settled on the reflectors, decreasing their reflectivity. 29 March 2017 was also a cloudy day, while 30 March 2017 was cloudy with rain, which would have resulted in increased diffused irradiance and less overall energy absorbed. The rain also caused dirt to settle on the plexiglass covers of the concentrators.

The small PV panel that powers the circulation pump is placed over the aperture of one of the concentrators, blocking light from reaching the reflector there, leading to less absorbed energy. The small gap loss created by inserting a radius on the CPC profile, while not very significant, would also contribute to less energy being absorbed.

As shown in Figure 46 and Figure 47, temperatures of over 90°C were achieved. Thus, the goal of this study was achieved.

Figure 50: Graph comparing the actual and theoretical cumulative useful energy gain for a cloudy day on 29 March

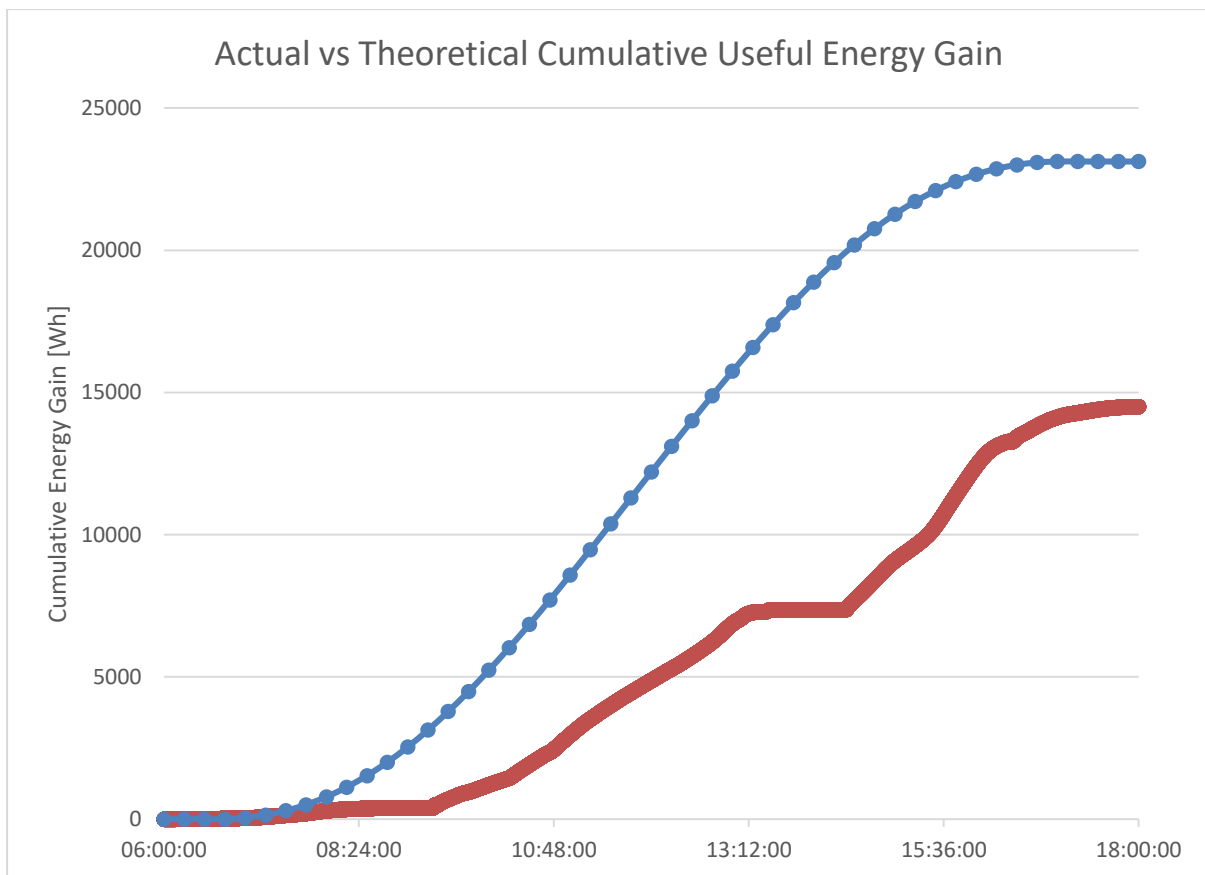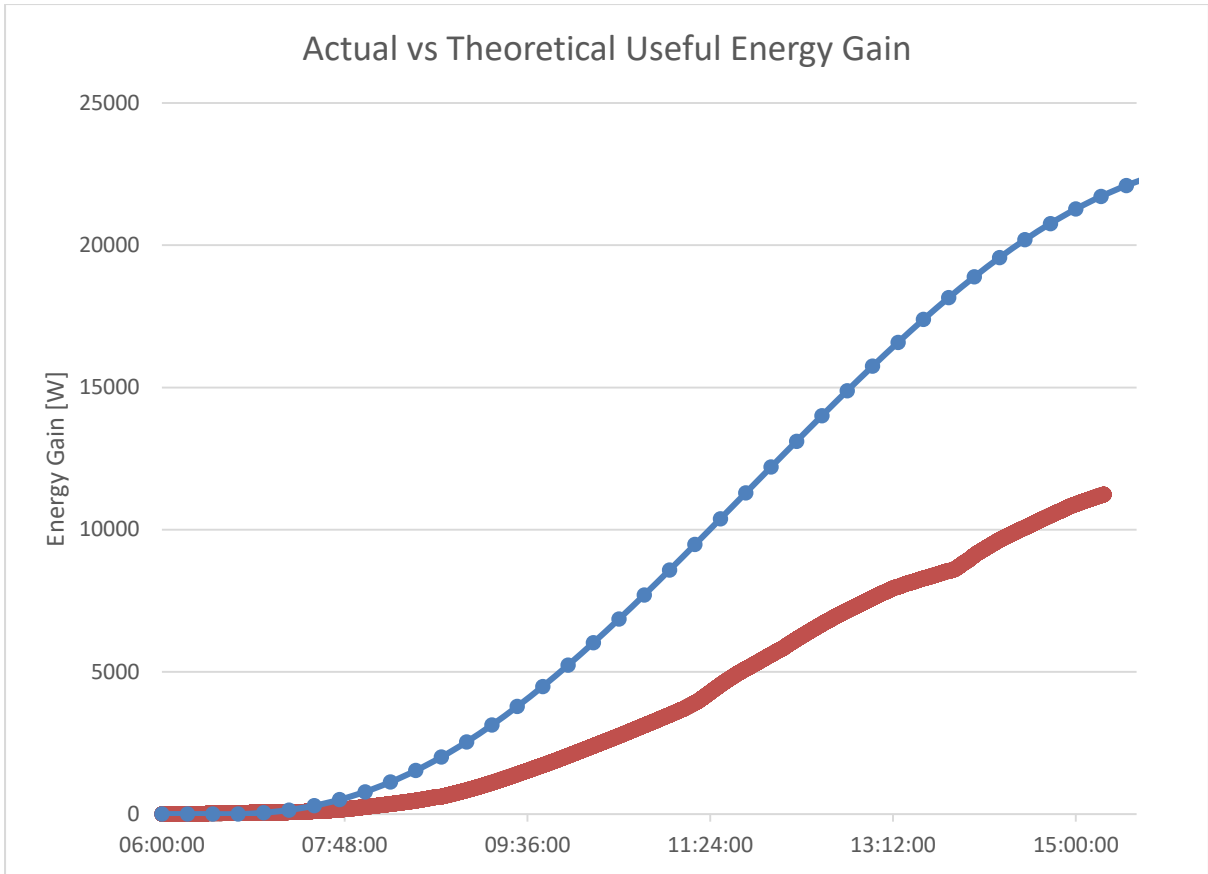**Figure 51: Graph comparing the actual and theoretical cumulative useful energy gain for a cloudy day on 30 March**

9   Conclusions and recommendations

The need for heating and cooling was reviewed and the inner workings of an absorption refrigeration system was discussed, including the operational needs op a bubble pump generator. Solar energy was discussed as an option to provide energy to the bubble pump and different types of solar collectors were reviewed.

A compound parabolic concentrator (CPC) was chosen as a suitable generator heat source due to its achievable temperatures, cost, efficiency and simplicity. Flat plate collectors (FPCs) were eliminated as a heat source, due to their achievable temperatures being too low, without making expensive design choices. Evacuated tube concentrators (ETCs) were eliminated due to their expensive materials and construction methods. Though parabolic trough collectors (PTCs) would provide an adequate temperature, the sun-tracking required to do so is too precise and expensive.

A literature survey was carried out to determine what studies have been done on CPCs and CPCs for use in aqua-ammonia refrigeration systems. Only one of the studies focused on South Africa as the location, and no studies applied sun-tracking to the CPCs used in aqua-ammonia absorption refrigeration systems.

Theory regarding how a CPC profile is formed, the position of the sun in the sky and how to describe its path using solar angles, and the thermal analysis of a CPC was given.

A mathematical model was then developed including considerations for solar angles, the profile of a CPC, sun-tracking angles with regards to the CPC profile, solar radiation data, and finally defined by the thermal analysis of a CPC.

In the collector design, the various components present in the design was discussed, including the CPC unit, the mechanical tracking system that incorporates a pendulum, escapement and gear train, and the crank mechanism for rotating the CPC units. An overview of the overall design was given and other fabrication considerations were discussed.

An experimental setup was then tested. The equipment used was discussed and a description of the test setup and conditions was given. Inlet, outlet and ambient temperatures, as well as the fluid flow rate was measured and logged.

A maximum temperature of about 109°C was achieved on a cloudy day, with the resultant maximum useful energy gain at 4462.33 W. Graphs were also created to compare the cumulative theoretical and experimental values, which showed a clear correlation. While the actual energy gain is less than the theoretical energy gain, reasons are given to explain the losses in energy.

It can then be accepted that the designed collector will be able to provide a temperature of 90°C to the aqua ammonia absorption refrigeration system's bubble pump, and that the model developed to predict the approximate energy gain is accurate.

It is recommended that an electronic system be investigated that is able to adjust the flow rate by considering the solar radiation input as well as the output temperature that is needed at any specific time. Such a system would optimize the solar collector output and simplify the needs of the bubble pump generator.

It would also be advantageous to convert the tracking method from purely mechanical to electronic, with servos rotating each CPC unit according to the exact solar altitude angle, allowing more radiation to be absorbed. This would simplify the tracking system, eliminating the need for so many moving components, however, a method of delivering electricity to this system would have to be investigated and would likely have to include either more solar PV panels and batteries or a generator running with fuel.

It is also recommended that, should any further study be done on a solar collector for this specific aqua-ammonia absorption refrigeration system, the testing only be done once the entire system has been assembled and installed. This would give a better understanding of how the components work together in reality, and of what is needed from the solar collector.

References

Adsten, M., Helgesson, A. & Karlsson, B. 2005. Evaluation of CPC-collector designs for stand-alone, roof- or wall installation. *Solar Energy*, 79(2005):638-647.

Aghbalou, F., Mimet, A., Badia, F., Illa, J., El Bouardi, A. & Bougard, J. 2004. Heat and mass transfer during adsorption of ammona in a cylindrical adsorbend bed: thermal performance study of a combined parabolic solar collector, water heat pipe and adsorber generator assembly. *Applied Thermal Engineering*, 24(2004):2537-2555.

Alternative Energy Tutorials. s.a. Parabolic Trough Reflector. http://www.alternative-energy-tutorials.com/solar-hot-water/parabolic-trough-reflector.html Date of access: 11 June 2015.

Casperson, J.R. 2011. Concentrating solar collector. (Patent: US 8058456 B1).

Eskom. 2015. Eskom to implement stage 1 load shedding this morning. Media release. 28 January. Eskom. s.l. http://www.eskom.co.za/news/Pages/LS4_15.aspx Date of access: 12 June 2015.

Farouk Kothdiwala, A., Norton, B. & Eames, P.C. 1995. The effect of variation of angle of inclination on the performance of low-concentration-ratio compound parabolic concentrating solar collectors. *Solar Energy*, 55(4):301-309.

Florides, G.A., Kalogirou, S.A., Tassou, S.A. & Wrobel, L.C. 2002. Modelling, simulation and warming impact assessment of a domestic-size absorption solar cooling system. *Applied Thermal Engineering*, 22(2002):1313-1325.

Garrison, J.D., Duff, W.S., O'Gallagher, J.J. & Winston R. 1993. Optimal non imaging integrated evacuated solar collector. *SPIE*, 2016:128-136.

GGHS (Go Green Heat Solutions). 2011. Flat plate collector. http://gogreenheatsolutions.co.za/?q=project-type/solar-water-heating/flat-plate-collector Date of access: 10 June 2015.

Gudekar, A.S., Jadhav, A.S., Panse, S.V., Joshi, J.B. & Padit, A.B. 2012. Cost effective design of compound parabolic collector for steam generation. *Solar Energy*, 90(2013):43-50.

Hsieh, C.K. 1983. Empirical equations for calculation of CPC collector loss coefficients. *Solar Energy*, 30(5):487-489.

Huld, T., Müller, R. & Gambardella, A. 2012. A new solar dariation database for estimating PV performance in Europe and Africa. *Solar Energy*, 86(2012):1803-1815.

Kalogirou, S.A. 2009. Solar energy engineering: Processes and systems. San Diego, CA. Elsevier.

Khalifa, A.N. & Al-Mutawalli, S.S. 1996. Effect of two-axis sun tracking on the performance of compound parabolic concentrators. *Energy Covers. Mgmt*, 39(10):1073-1079.

Kim, Y., Han, G. & Seo, T. 2007. An evaluation on thermal performance of CPC solar collector. *International Communications in Heat and Mass Transfer*, 35(2008):446-457.

Kim, Y.S., Balkoski, K., Jiang, L. & Winston, R. 2013. Efficient stationary solar thermal collector systems operating at a medium-temperature range. *Applied Energy*, 111(2013):1071-1079.

Lambert, M.A. 2006. Design of solar powered adsorption heat pump with ice storage. *Applied Thermal Engineering*, 27(2007):1612-1628.

Li, X., Dai, Y.J., Li, Y. & Wang, R.Z. 2013. Comparative study on two novel intermediate temperature CPC solar collectors with the U-shape evacuated tubular absorber. *Solar Energy*, 93(2013):220-234.

Lu, Z.S., Wang, R.Z., Xia, Z.Z., Lu, X.R., Yang, C.B., Ma, Y.C. & Ma, G.B. 2013. Study of a novel solar adsorption cooling system and solar absorption cooling system with new CPC collectors. *Renewable Energy*, 50(2013):299-306.

Mehalic, B. 2009. Flat-plate & evacuated-tube solar thermal collectors. http://www.homepower.com/articles/solar-water-heating/equipment-products/flat-plate-evacuated-tube-solar-thermal-collectors Date of access: 11 June 2015.

Moodaly, A. 2008. The modelling of solar radiation quantities and intensities in a two dimensional compound parabolic collector. University of Johannesburg. (Dissertation – Meng).

Ortega, N., Garcia-Valladares, O., Best, R. & Gomez, V.H. 2007. Two-phase flow modelling of a solar concentrator applied as ammonia vapor generator in an absorption refrigerator. *Renewable Energy*, 33(2008):2064-2076.

Potgieter, M.C. 2013. The evaluation of a solar-driven aqua-ammonia diffusion absorption heating and cooling cycle. Potchefstroom: NWU. (Dissertation - MEng).

Rivera, C.O. & Rivera, W. 2003. Modeling of an intermittent solar absorption refrigeration system operating with ammonia-lithium nitrate mixture. *Solar Energy Materials & Solar Cells*, 76(2003):417-427.

Rivera, W., Moreno-Quintanar, G., Rivera, C.O., Best, R. & Martinez, F. 2010. Evaluation of a solar intermittent refrigeration system for ice production operating with ammonia/lithium nitrate. *Solar Energy*, 85(2011):38-45.

Rönnelid, M. & Karlsson, B. 1996a. Experimental Investigation of heat losses from low-concentrating non-imaging concentrators. *Solar Energy*, 57(2):99-109.

Rönnelid, M., Perers, B. & Karlsson, B. 1996b. Construction and testing of a large-are CPC-colletor and comparison with a flat plate collector. *Solar Energy*, 57(3):177-184.

SolarGIS. 2013. Maps of direct normal irradiation (DNI). http://solargis.info/doc/free-solar-radiation-maps-DNI Date of access: 4 March 2015.

Srikhirin, P. & Aphornratana, S. 2002. Investigation of a diffusion absorption refrigerator. *Applied Thermal Engineering*, 22(11):1181-1193.

Stoecker, W.F. & Jones, J.W. 1983. Refrigeration and air conditioning. 2nd ed. New York City, NY: McGraw Hill, Inc.

Su, Y., Riffat, S.B. & Pei, G. 2012. Comparitive study on annual solar energy collection of a nover lens-walled compound parabolic concentrator (lens-walled CPC). *Sustainable Cities and Society*, 4(2012):35-40.

Tamainot-Telto, Z. & Critoph, R.E. 1999. Solar sorption refrigerator using a CPC collector. *Renewable Energy*, 16(1999):735-738.

Tang, R. & Yu, Y. 2010. Feasibility and optical performance of one axis three positions sun-tracking polar-axis aligned CPCs for photovoltaic applications. *Solar Energy*, 84(2010):1666-1675.

Tiba, C. & Fraidenraich, N. 2011. Optical and thermal optimization of stationary non-evacuated CPC solar concentrator with fully illuminated wedge receivers. *Renewable Energy*, 36(2011):2547-2553.

Van Der Walt, S. 2012. The design and optimisation of a bubble pump for an aqua-ammonia diffusion absorption heat pump. Potchefstroom: NWU. (Dissertation - MEng).

Wang, Y.F., Zhu, Y.Z., Chen, H.J., Zhang, X., Yang, L. & Liao, C.H. 2015. Performance analysis of a novel sun-tracking CPC heat pipe evacuated tubular collector. *Applied Thermal Engineering* (In Press).

White, S.J. 2001. Bubble pump design and performance. Georgia Institute of Technology. (Dissertation - MEng).

Winston, R., Minano, J.C. & Benitez, P. 2005. Nonimaging Optics. San Diego, CA. Elsevier.

Winston, R., Jiang, L. & Widyolar, B. 2013. Performance of a 23KW solar thermal cooling system employing a double effect absorption chiller and thermodynamically efficient non-tracking concentrators. *Energy Procedia*, 48(2014):1036-1046.

Yadav, Y.P., Yadav, A.K., Anwar, N., Eames, P.C. & Norton, B. 1996. The fabrication and testing of a line-axis compound parabolic concentrating solar energy collector. *WREC 1996*, 572-575.

Bibliography

Goodrich, W.L. 1905. The Modern Clock: A Study of Time Keeping Mechanism; Its Construction, Regulation and Repair. Chicago, IL. Hazlitt & Walker, Publishers.

Lund, H. 2010. Renewable Energy Systems: The Choice and Modelling of 100% Renewable Systems. San Diego, CA. Elsevier.

Mathhys, R.J. 2004. Accurate Clock Pendulums. New York, NY. Oxford University Press.

Mousazadeh, H., Keyhani, A., Javadi, A., Mobli, H., Abrina, K. & Ahmad, S. 2009. A review of principle and sun-tracking methods for maximizing solar systems output. *Renewable and Sustainable Energy Reviews*, 13(2009):1800-1818.

Appendix A – EES code used for verification

```
D_o = 0,0318
t = 0,003
D_i = D_o - 2 * t
A_a = 9,835526249
A_r = 4,699420486
C = 2,092923219

Nu = 4,364
k = 53,661
k_f = 0,1362
epsilon_abs = 0,65
tau_cover = 0,85
alpha_r = 0,96
rho = 0,9
n = 0,6

h_f = (Nu * k_f) / D_i
tau_CPC = rho^n

"G = 723
G_d = 173
T_a = 28
T_i = 63"
T_o = 105
m_dot = 0,03
c_p = 2188

U_L = (0,18 + 16,95 * epsilon_abs) * (0,212 + 0,00255 * T_a + (0,00186 + 0,000012 * T_a) * (((T_o - T_i) / 2) - T_a))

F_acc = (1 / U_L) / ((1 / U_L) + (D_o / (h_f * D_i)) + ((D_o / (2 * k)) * (ln(D_o / D_i))))

F_R = ((m_dot * c_p) / (A_a * U_L)) * (1 - exp(-((U_L * F_acc * A_a) / (m_dot * c_p))))

gamma = 1 - (1 - 1 / C) * (G_d / G)

S = G * tau_cover * tau_CPC * alpha_r * gamma

Q_u = F_R * (S * A_a - A_r * U_L * (T_i - T_a))

"Month = 1"
```